NASA CR-134543

PARTICLE FLOW IN BLADE PASSAGES OF TURBOMACHINERY WITH APPLICATION TO LASER-DOPPLER VELOCIMETRY

by

Barry R. Maxwell

prepared for

NATIONAL AERONAUTICS AND SPACE ADMINISTRATION

NASA NGR-39-027-002

BUCKNELL UNIVERSITY
LEWISBURG, PENNSYLVANIA

Requests for copies of this report should be referred to

National Aeronautics and Space Administration
Office of Scientific and Technical Information
Attention: AFSS-A
Washington, D.C. 20546

1. Report No.	2. Government Accession No.	3. Recipient's Catalog No.
NASA CR-134543		

4. Title and Subtitle	5. Report Date
PARTICLE FLOW IN BLADE PASSAGES OF TURBOMACHINERY WITH APPLICATION TO LASER-DOPPLER VELOCIMETRY	February 1974
	6. Performing Organization Code
7. Author(s)	8. Performing Organization Report No.
Barry R. Maxwell	
9. Performing Organization Name and Address	10. Work Unit No.
Bucknell University Lewisburg, PA 17837	11. Contract or Grant No. NGR-39-027-002
	13. Type of Report and Period Covered Contractor Report
12. Sponsoring Agency Name and Address	14. Sponsoring Agency Code
National Aeronautics and Space Administration Washington, DC 20546	

15. Supplementary Notes

Project Manager, Richard G. Seasholtz, Physical Science Division, NASA Lewis Research Center, Cleveland, OH

16. Abstract

A theoretical analysis was conducted of the dynamic behavior of micron size particles entrained in gas flow on the two-dimensional blade-to-blade surface of a circular stationary cascade of turbine stator blades. The particle velocity lag and angular deviation relative to the gas was determined as a function of particle diameter and mass density. Particle size and density were varied over ranges selected to correspond to typical laser-Doppler velocimeter (LDV) flow field mapping applications. It was found that velocity lag and angular deviation increased whenever particle size or mass density increased, and that particle tracking was more sensitive to a change in particle diameter than to a change in mass density. Results indicated that LDV applications employing 1 gm/cc tracer particles with diameters greater than approximately 1 micron, or 0.5 micron diameter particles with mass densities greater than 4 gm/cc would experience velocity and angular deviations generally greater than 2 percent and 1 degree, respectively.

17. Key Words (Suggested by Author(s))	18. Distribution Statement
Laser-Doppler Velocimetry Particle Flow Turbomachinery	Unclassified-unlimited

19. Security Classif. (of this report)	20. Security Classif. (of this page)	21. No. of Pages	22. Price*
Unclassified	Unclassified	~~34~~ 42	$3.00

NASA CR-134543

FINAL REPORT

PARTICLE FLOW IN BLADE PASSAGES OF TURBOMACHINERY WITH APPLICATION TO LASER-DOPPLER VELOCIMETRY

by

Barry R. Maxwell

prepared for

NATIONAL AERONAUTICS AND SPACE ADMINISTRATION

January 31, 1974

NASA GRANT NGR-39-027-002

Technical Management
NASA Lewis Research Center
Cleveland, Ohio
Physical Science Division
Richard G. Seasholtz

BUCKNELL UNIVERSITY
Lewisburg, Pennsylvania 17837

TABLE OF CONTENTS

ABSTRACT	iv
NOMENCLATURE	v
LIST OF FIGURES	vi
INTRODUCTION	1
GAS-PARTICLE FLOW SYSTEM	3
GOVERNING EQUATIONS AND ANALYSIS	4
PARTICLE FLOW	5
PARAMETRIC STUDY	7
GAS FLOW RESULTS	9
PARTICLE FLOW RESULTS AND DISCUSSION	10
CONCLUSIONS	13
REFERENCES	15
FIGURES	18-34

ABSTRACT

A theoretical analysis was conducted of the dynamic behavior of micron size particles entrained in gas flow on the two-dimensional blade-to-blade surface of a circular stationary cascade of turbine stator blades. The particle velocity lag and angular deviation relative to the gas was determined as a function of particle diameter and mass density. Particle size and density were varied over ranges selected to correspond to typical laser-Doppler velocimeter (LDV) flow field mapping applications. It was found that velocity lag and angular deviation increased whenever particle size or mass density increased, and that particle tracking was more sensitive to a change in particle diameter than to a change in mass density. Results indicated that LDV applications employing 1 gm/cc tracer particles with diameters greater than approximately 1 micron, or 0.5 micron diameter particles with mass densities greater than 4 gm/cc would experience velocity and angular deviations generally greater than 2 percent and 1 degree, respectively.

NOMENCLATURE

b	stream-channel thickness normal to meridional streamline
C_D	drag coefficient
$\dot{m}$	mass flow rate of gas through stream channel
M	Mach number
r	particle radius
R	radius from axis of rotation to meridional stream-channel mean line
Re	Reynolds number, $2r\rho_g\|U-V\|\mu$
T	temperature
U	gas velocity
V	particle velocity
X	meridional streamline distance
α	angle between meridional streamline and axis of rotation
β	flow angle measured relative to meridional direction
γ	ratio of specific heats
Θ	tangential coordinate
$\bar{\Theta}$	normalized tangential coordinate
μ	gas viscosity
ρ	density
ϕ	absolute angular deviation between the particles and gas, $\|\beta_p-\beta_g\|$
ψ	stream function
	Subscripts
g	gas
p	particles
x	meridional direction
Θ	tangential direction

LIST OF FIGURES

FIGURE	TITLE	PAGE
1	Blade-To-Blade Surface of Revolution	18
2	Blade-To-Blade Solution Region	19
3	Gas Flow Velocity Profiles Across Stream Channel, $\dot{m} = 6.68 \times 10^{-3}$ lb/sec, $\rho_g = 7.403 \times 10^{-2}$ lb/ft^3, T = 523.7 R, $\gamma = 1.4$	20
4	Gas Flow Angle Profiles Across Stream Channel, $\dot{m} = 6.68 \times 10^{-3}$ lb/sec, $\rho_g = 7.403 \times 10^{-2}$ lb/ft^3, T = 523.7 R, γ 1.4	21
5	Particle Trajectories Through the Solution Region	22
6	Particle Trajectories as a Function of Particle Radius	23
7	Particle Trajectories as a Function of Particle Mass Density	24
8	Tangential Variation of Particle-To-Gas Velocity Ratio with Particle Radius as a Parameter, $\rho_p = 1$ gm/cc	25
9	Tangential Variation of Particle-To-Gas Velocity Ratio with Particle Mass Density as a Parameter, r = 0.25 micron	26
10	Tangential Variation of Angular Deviation with Radius as a Parameter, $\rho_p = 1$ gm/cc	27
11	Tangential Variation of Angular Deviation with Particle Mass Density as a Parameter, r = 0.25 micron	28
12	Contours of Constant Particle-To-Gas Velocity Ratio, $\rho_p = 1$ gm/cc	29-31
13	Contours of Constant Angular Deviation, $\rho_p = 1$ gm/cc	32-34

INTRODUCTION

Laser-Doppler velocimetry (LDV) is a noncontact, optical technique for determining the velocity of flowing fluids by measuring the velocity of tracer particles entrained in the fluid rather than by measuring the velocity of the fluid itself. The LDV technique is of considerable importance in gas dynamic measurements because it is unnecessary to introduce any hardware into the flow system. Because of the absence of a physical probe, the LDV technique is ideally suited to measuring gas velocities in the flow passages between rotor and stator blades of turbomachines. Development of noncontact velocimetry techniques in turbomachinery will provide data currently required to extend and improve design methods, blade performance, and efficiency of components used in advanced airbreathing engines. It is for this reason that the LDV technique is beginning to find application in the aircraft turbomachinery field.[1,2]

The laser-Doppler velocimeter system measures only the motion of micron size naturally occurring or artificially generated tracer particles entrained in the fluid, and its accuracy is, therefore, limited by the accuracy with which the particles follow the fluid flow. Since it is important to know how accurately the particles track the fluid flow, careful consideration must be given throughout the flow region to the magnitude and direction of the particles velocity relative to the carrier fluid velocity. This paper documents a theoretical investigation of the dynamic behavior of micron size particles entrained in gas flow on the two-dimensional blade-to-blade surface of a circular stationary cascade of turbine stator blades. The particle velocity lag and angular deviation relative to the gas are determined as a

function of particle size and mass density. Information of this nature is currently required for the application of LDV techniques to the intrablade flow field mapping of aircraft turbomachinery.

Several previous studies [3-5] have investigated particle tracking for LDV applications but have been restricted to particle flow in such systems as turbulent flows, nozzles, oscillating gases, shock waves, and over airfoils. Reference 6 used a LDV system to measure the velocity lag of aerosol particles in small supersonic nozzles and then used this information in conjunction with numerical predictions to determine particle size. A theoretical study by Hussein and Tabakoff [7] and an experimental study of Tabakoff et al.[8] provide trajectories and velocities of solid particles suspended in a gas passing through an axial flow turbine stage. The objective of their investigations was to estimate the flow properties of a gas-particle suspension flowing over turbine blades. This information would ultimately be used to minimize blade erosion, through appropriate redesign. Since their work considered particle sizes generally ranging from 100-900 microns, their results are inapplicable for LDV applications because of the resulting high velocity lags. Wisler and Mossey[2] obtained detailed flow field measurements within the rotating blade row of a low speed axial compressor using a laser-Doppler velocimeter. Their measurements generally agreed to within 2-3 percent with hot film and pitot-static probe measurements outside the blade row, and with potential flow solutions near the leading edge. Their work was restricted however, to flow velocities sufficiently low that particle velocity lag was not regarded as a significant problem. However, as gas flow velocities and accelerations increase, particle velocity lag in blade channels becomes more significant and application of LDV techniques to flow field analysis

should be guided by the results of a dynamic analysis of similar gas-particle flow systems.

GAS-PARTICLE FLOW SYSTEM

The flow system analyzed in this study is the gas-particle flow on the mean blade-to-blade surface of a circular stationary cascade of turbine stator blades. The cascade was designed for cooled-turbine thermodynamic studies and is currently undergoing testing at the NASA Lewis Research Center. It has 72 blades and each blade has a 3.85 in. span and 2.47 in. chord. The tip diameter of the turbine is 31.9 in.; the hub-to-tip radius ratio is .76 and the mean radius solidity is 2.05. Coorinates of the actual blade profile are given in ref. 9 for three radial sections. The flow is considered to be two-dimensional and the independent variables are the meridional streamline distance X and the tangential angle Θ. For purposes of analysis, a finite solution region is chosen on the blade-to-blade surface. It is bounded on the top and bottom by adjacent blade surfaces, and by upstream and downstream boundaries along which the flow is assumed to be uniform. The blade-to-blade surface of revolution, solution region, and coordinate system employed are shown in fig. 1. A stream channel is defined by specifying a meridional streamline radius R and a stream-channel thickness b at several meridional locations. The streamline radius and stream-channel thickness are R=1.16773 feet and b=.0031939 feet, respectively, and remained constant (to within 1 percent) throughout the solution region. The blade-to-blade solution region and the grid used for finite-difference analysis of the governing equations is shown in figure 2.

GOVERNING EQUATIONS AND ANALYSIS

Analysis of the gas-particle flow field was conducted in two steps. In the first, the magnitude and direction of the gas velocity was determined at all interior grid points of the blade-to-blade solution region. In the second step, the magnitude and direction of the particle velocity was determined throughout the region by analyzing the path followed by particles in a two-dimensional flow field with a known gas velocity distribution. Decoupling the gas and particle flows in this way is justified because of the low mass fraction of naturally occurring or artificially generated aerosols in most LDV gas-dynamic applications. Therefore, the particles do not influence the gas flow, and the particles and gas may be analyzed separately.

GAS FLOW

The gas flow field in the blade-to-blade solution region was determined with a solution method developed by Katsanis[10]. The method yields a two-dimensional, isentropic, shock free, transonic flow solution on a blade-to-blade surface on which the flow is essentially subsonic. The solution is obtained by a combination of a finite-difference stream-function solution and a velocity gradient solution. The simplifying assumptions used in formulating the governing equation are: (a) the fluid is a perfect gas and is nonviscous, (b) the flow is steady and irrotational (c) the velocity component normal to the solution surface is zero, (d) the magnitude and direction of the velocity are uniform across the upstream and downstream boundaries, (e) the only forces acting on the fluid are those due to momentum and the pressure gradient, and (f) the total energy of the system remains constant.

The conservation of momentum equation for a compressible, non-viscous fluid in steady flow through a stationary cascade is given[10] in terms of the stream function ψ as:

$$\frac{\partial^2\psi}{\partial x^2} + \frac{1}{R^2}\frac{\partial^2\psi}{\partial\theta^2} - \frac{1}{R^2\rho_g}\frac{\partial\rho_g}{\partial\theta}\frac{\partial\psi}{\partial\theta} + \frac{\partial\psi}{\partial x}\left[\frac{\sin\alpha}{R} - \frac{1}{b\rho_g}\frac{\partial}{\partial x}(b\rho_g)\right] = 0 \qquad (1)$$

where

$$U_x = \frac{\dot{m}}{Rb\rho_g}\frac{\partial\psi}{\partial\theta}$$

$$U_\theta = \frac{\dot{m}}{b\rho_g}\frac{\partial\psi}{\partial x}$$

The stream function is 0 on the upper surface of the lower blade (suction surface) and 1 on the lower surface of the upper blade (pressure surface). For flow systems in which the flow is everywhere subsonic, the solution to eqn. (1) can be obtained with a finite-difference approach. However, if there is locally supersonic flow, the solution is obtained by a velocity-gradient method using information obtained from a finite-difference solution of eqn. (1) at a reduced weight flow. The derivation of the velocity-gradient equation and details of the solution precedure are given in ref 10.

PARTICLE FLOW

The differential equation of motion in vector form of a single, spherical particle immersed in a fluid in the absence of potential force fields is

$$\frac{4}{3}\pi r^3\rho_p\frac{D\bar{V}}{Dt} = C_D\frac{\pi r^2}{2}\rho_g(\bar{U}-\bar{V})|\bar{U}-\bar{V}| \qquad (2)$$

The term on the left denotes the mass times the acceleration of the particle, and, therefore represents the force required to accelerate the particle. The term on the right represents the total viscous drag exerted on the particle by the surrounding fluid and is expressed in terms of an empirically determined viscous drag ceofficient C_D. Equation (2) assumes that the force on the particle caused by the pressure gradient in the surrounding fluid, the force required to accelerate the apparent mass of the particle relative to the fluid, and the force which accounts for the deviation of the flow from steady state (Basset force) are negligible. These assumptions are justified [5,7] in flow systems whose properties are changing very gradually or when the particle density is much larger than the fluid density. Both of these conditions are satisfied in this study. It is also assumed that the particles are non-interacting and uniformally distributed within the carrier gas, and that there are sufficiently few particles that their presence does not alter the gas properties from that of the gas flow alone. These assumptions are valid for most LDV applications employing naturally occurring or artifically generated aerosols. The steady-state meridional and tangential components of eqn. (2) become

$$\frac{dV_x}{dx} = \frac{3C_D\rho_g}{8r\rho_p V_x}(\bar{U}_x-\bar{V}_x)|U-V| \qquad (3)$$

$$\frac{dV_\theta}{d\theta} = \frac{3C_D\rho_g}{8r\rho_p V_\theta}(U_\theta-V_\theta)|U-V| \qquad (4)$$

The path followed by a particle and its velocity along that path may be determined by numerically integrating eqns. (3) and (4) in an interative manner throughout the gas flow field.

Numerical integration is required because of the nonlinear nature of the empirically determined drag coefficient. Since the gas flow is assumed not to have a radial velocity component, the particles also do not have one, and are, therefore, constrained to remain in the stream channel defined by the meridional radius R and the stream-channel thickness b.

In the absence of reliable drag data the drag coefficient is frequently assumed to be given by the classical Stokes drag law $C_D = 24/Re$, where $Re = 2rp_g|U-V|/\mu$. Although it is most convenient to use Stokes law for the drag coefficient, it becomes increasingly unrealistic for Reynolds numbers above approximately 1.0 and in flows where rarefaction, compressibility and inertial effects are significant. The drag coefficient used in this study is given by Carlson and Hoglund[11] and corrects the Stokes law for these effects. Therefore, it is applicable throughout the continuum, slip and transition flow regimes. The expression is

$$C_D = \frac{24}{Re}\left[\frac{(1+.15\,Re^{.687})(1+\exp(-.427/M^{4.65}-3/Re^{.88}))}{1+(M/Re)(3.82+1.28\exp(-1.25\,Re/M))}\right] \qquad (5)$$

where the term in the bracket accounts for deviation from Stokes flow. The Mach number is based upon the absolute relative velocity of the gas with respect to the particles.

PARAMETRIC STUDY

The dynamic behavior of several gas-particle mixtures was determined by numerically solving eqns. (3) and (4) in an interative manner for the particle velocity components. The viscous drag coefficient is given by eqn (5). Several cases were examined by varying the size and

mass density of the particles over ranges selected to correspond to values encountered in most LDV gas dynamic applications. The particle radius varied from 0.5 - 2 microns, and the mass density ranged from 1-4 gm/cc. The gas flow remained constant throughout the study and was characterized by a mass flow rate, $\dot{m} = 6.68 \times 10^{-3}$ lb/sec, mass density, $\rho_g = 7.403 \times 10^{-2}$ lb/ft^3, inlet temperature equal to 523.7 R, and a specific heat ratio γ=1.40. The gas flow entered the solution region with an inlet flow angle of zero relative to the meridional direction and an average velocity of 285.4 ft/sec. Particles were introduced into the solution region at several locations along the upstream boundary. They were assumed to possess a velocity equal to 99 percent of the corresponding gas velocity at that point, and have no angular deviation relative to the gas. Their trajectories and velocities were numerically determined as they progressed through the region. Analysis of a particular particle was continued until either it passed out of the solution region or until it entered the near-blade region. This region is defined as the area between the finite-difference grid network and a blade surface. Since particles which entered this region were generally large and dense, and therefore unsuitable for LDV applications, their analysis was terminated immediately after entering the region. In an actual blade channel, particles which enter the near blade region normally collide with the adjacent blade surface and rebound back into the flow stream with an increased velocity lag and angular deviation relative to the gas. In practice, LDV electronics systems are generally designed to descriminate against such particles either because of their large size or because their velocities are significantly different from the mean velocity of surrounding particles.

GAS FLOW RESULTS

The results of numerically integrating eqn. (1) through the solution region of figure 2 are shown in figures 3 and 4. Figure 3 presents the tangential variation of the gas velocity magnitude at several meridional locations. Tangential profiles were determined along every vertical grid line of figure 2; however, in order to minimize confusion, only profiles at ¼ inch increments have been plotted. Since the tangential limits of each velocity profile on figure 3 corresponds to the limits of its grid reference line of figure 2, the two figures must be used in conjunction with each other to determine the meridional position of each profile. In general, the profiles progress from the upper left to the lower right as the meridional stream length increases. Each intrablade profile includes the blade surface velocity as its limit points. The results indicate that the velocity on the suction side is generally greater than the pressure side, at the same meridional position, and that the flow is generally well behaved except for local flow reversals near the trailing edge of the upper blade. The intrablade Mach numbers range from 0.125 - 0.891.

Tangential profiles of the angle of the gas velocity vector are presented in figure 4 at the same meridional positions as figure 3. Flow angles are measured from the meridional direction. Flow approaching the blade channel is represented by the profiles on the upper right portion of figure 4, and the profiles progress downward and to the left as the meridional streamlength increases. It's seen that the gas leaves the flow region at an angle of approximately -62.5 degrees, and that the flow angle is relatively insensitive to the tangential position in the channel except near the leading and trailing edges of the blade channel.

PARTICLE FLOW RESULTS AND DISCUSSION

The results of numerically integrating eqns. (3) and (4) through the solution region are summarized in figures 5-13. Figure 5 presents several trajectories of 1 micron diameter particles with a mass density of 1 gm/cc. The trajectories are typical of those obtained throughout the study and represent the approximate range of trajectories examined which did not intersect either the upper or lower near-blade region. The partial trajectories shown downstream from the blades are those of particles which pass through the blade channel directly above the one investigated.

The influence of particle radius and mass density is shown in figures 6 and 7, respectively. An increase in either parameter causes an extension, or lagging, of the trajectory and this results in a corresponding increase in the velocity lag and angular deviation between the particles and the gas. While the results shown are for a particle mass density and diameter of 1 gm/cc and 0.5 micron, respectively, the results are typical of all other cases examined. It's seen that the particle path is more sensitive to an increase in radius than to a corresponding increase in mass density. This is justified by noting from eqns. (3) and (4) that if Stokes flow prevailed ($C_D = 24/Re$), then ρ_p would appear to the first power in the denominator of both right hand terms and the particle radius would appear to the second power. Under these conditions a doubling of the particle size would have the same effect on the trajectory as a 4 to 1 increase in mass density. While Stokes flow does not always occur in this study, the above analogy remains essentially valid since the drag expression given by eqn. (5) is based upon the Stokes drag law.

The tangential variation of particle velocity ratio and particle angular deviation at several meridional positions is illustrated in figures 8-11 as a function of particle radius and mass density. The abscissa is the normalized tangential position and is 0 at the suction surface and 1 at the pressure surface. Particle velocity ratio is defined as the magnitude ratio of the particle velocity to gas velocity V/U, and particle angular deviation ϕ is defined as $\phi = |\beta_p - \beta_g|$. These parameters characterize the dynamic behavior of a particle at a particular point in a fluid flow. Particle velocity lag is defined as $|U-V|/U$ and is a related alternate parameter. Such a parameter does not, however, indicate whether the particles are moving faster or slower than the surrounding gas. LDV applications typically require that $.99 \leq V/U \leq 1.01$ and $\phi < .5$ degree. The tangential profiles of V/U and ϕ do not extend the full tangential height of the stream channel because of intersection of the outer trajectories with the near-blade region and the channeling of trajectories with increasing meridional streamlength and particle radius. The channeling effect is particularly evident in figures 8 and 10.

The results indicate that an increase in either particle radius or mass density causes an increase in velocity lag and angular deviation. As figures 6 and 7 suggested, particle tracking is more sensitive to particle radius than to mass density. Figures 8-11 indicate that doubling the particle radius causes approximately the same change in V/U and ϕ throughout the region as a 4 to 1 increase in the mass density. Therefore, the particle trajectory would remain essentially unchanged if the particle diameter was halved while at the same time increasing its mass density by a factor of 4. The figures

also indicate that tracking is better in the region downstream from the blade channel than in the channel itself. This trend results from the deceleration of the gas in the latter portion of the stream channel (fig. 3) and the gradual catching-up of the particles relative to the gas. When X=2.26 in., figs. 8 and 9 indicate that in the region adjacent to the suction surface the particles are actually moving faster than the gas flow (V/U>1).

Figures 12 and 13 illustrate the tracking capability of three different size particles through the solution region. Tracking is graphically shown by lines of constant velocity ratio and angular deviation. The results indicate that the steepest gradients in V/U occur near the leading and trailing edges of the blade channel. The high leading edge gradient is caused by the sudden contraction of the blade channel in that region, and the high gradient just downstream from the blade channel is due to the sudden enlargement of flow area at the trailing edge.

The regions of greatest velocity lag occur generally in several well defined regions, or pockets. Two pockets are adjacent to the leading edges of the blades in the region of greatest curvature. Another pocket lies approximately two thirds of the way through the blade channel and adjacent to the pressure surface. Particles in these regions are moving slower than the gas and are attempting to catch-up. The remaining regions of high velocity lag are near the trailing edge of the upper blade surface and in the narrow, high V/U gradient region immediately downstream from the blade channel. Because of the gas deceleration in these regions, the particle velocity actually exceeds the gas velocity.

Minimum velocity lag generally occurs near the entrance to the flow region where the gas-particle mixture was introduced, and in a region just prior to the trailing edge of the channel where the particles have caught-up to the decelerating gas. Another favorable region is seen to lie in the narrow high gradient region downstream from the channel.

CONCLUSIONS

The results presented above have provided information regarding the dynamic behavior of micron size particles in the two-dimensional flow field between blades of a stationary turbine cascade. The results indicated that particle velocity lag and angular deviation is increased whenever particle size or mass density is increased, and that these tracking parameters are more sensitive to a change in particle radius than to a corresponding change in mass density. It was found that a 2 to 1 increase in particle diameter decreased particle trackability by approximately the same amount as a 4 to 1 increase in particle mass density. Therefore, a 0.5 micron diameter particle with a mass density of 4 gm/cc behaved essentially the same as a 1 micron particle with a mass density of 1 gm/cc. The greatest velocity lag occurs in several regions near the entrance and exit of the blade channel and the minimum lag occurs in the region of decelerating gas flow prior to the blade channel exit. Results indicate that LDV applications employing 1 gm/cc tracer particles with diameters greater than approximately 1 micron, or 0.5 micron diameter particles with mass densities greater than 4 gm/cc would experience velocity and angular deviations generally greater than 2 percent and 1 degree, respectively.

It should be emphasized that this study did not investigate particle flow in the boundary layers of the blade channel nor did it examine particle collision phenomena with the blade surfaces. Therefore, it is conceivable that there may be particles within the blade channel which have previously collided with a blade surface and possess a velocity and flow angle significantly different from the surrounding undeflected particles. Several cases were numerically investigated in which particles were introduced into the blade channel with velocities and flow angles significantly different from those of the surrounding gas. The results generally showed that particles below 1 micron in diameter and less than 4 gm/cc adjusted very rapidly to the gas flow field around them. The conclusion is that unless the particles are very large and dense, the dynamic behavior of blade impacted particles is essentially indistinguishable from the behavior of the surrounding undeviated particles.

REFERENCES

[1]Alwang, W., Cavanaugh, L., Burr, R., and Hauer, A., "Optical Techniques for Flow Visualization and Flow Field Measurements in Aircraft Turbomachinery," PWA-3942, June 1970, Pratt and Whitney Aircraft, Hartford, Conn.

[2]Wisler, D. C. and Mossey, P. W., "Gas Velocity Measurements Within a Compressor Rotor Passage Using the Laser Doppler Velocimeter," ASME Paper 72-WA/GT-2, New York, 1972.

[3]Yanta, W. J., Gates, David F., and Brown, F. W., "The Use of a Laser Doppler Velocimeter in Supersonic Flow," NOLTR 71-169, Aug. 1971, Naval Ordnance Laboratory, Silver Spring, Maryland.

[4]Karchmer, A. M., "Particle Trackability Considerations for Laser Doppler Velocimetry," TM X-2628, Sept. 1972, NASA.

[5]Maxwell, B. R. and Seasholtz, R. G., "Velocity Lag of Solid Particles in Oscillating Gases and in Gases Passing Through Normal Shock Waves," TN-D-7490, 1974, NASA.

[6]Yanta, W. J., "Measurements of Aerosol Size Distributions with a Laser Doppler Velocimeter (LDV)," AIAA Paper No. 73-705, 1973.

[7]Hussein, M. and Tabakoff W., "Three Dimensional Dynamic Characteristics of Solid Particles Suspended by Polluted Air Flow in a Turbine Stage," AIAA Paper No. 73-140, Wasington, D.C., 1973.

[8]Tabakoff, W., Hamed, A. and Hussein, M. F., "Experimental Investigation of Gas-Particle Flow Trajectories and Velocities in an Axial Flow Turbine Stage, ASME Paper No. 72-GT-57, New York, 1972.

[9]Gladden, H. J., Dengler, R. P., Evans, D. G., and Hippensteel, S. A., "Aerodynamic Investigation of Four-Vane Cascade Designed for Turbine Cooling Studies," TMX-1954, Jan. 1970, NASA.

[10]Katsanis, T., "Fortran Program for Calculating Transonic Velocities on a Blade-To-Blade Stream Surface of a Turbomachine," TN D-5427, Sept. 1969, NASA.

[11]Carlson, D. J. and Hoglund, R. F., "Particle Drag and Heat Transfer in Rocket Nozzles," AIAA J., Vol. 2, No. 11, November 1964, pp. 1980-94.

LIST OF FIGURE CAPTIONS

Figure 1 Blade-To-Blade Surface of Revolution

Figure 2 Blade-To-Blade Solution Region

Figure 3 Gas Flow Velocity Profiles Across Stream Channel, $\dot{m} = 6.68 \times 10^{-3}$ lb/sec, $\rho_g = 7.403 \times 10^{-2}$ lb/ft^3, T = 523.7 R, $\gamma = 1.4$

Figure 4 Gas Flow Angle Profiles Across Stream Channel, $\dot{m} = 6.68 \times 10^{-3}$ lb/sec, $\rho_g = 7.403 \times 10^{-2}$ lb/ft^3, T = 523.7 R, $\gamma = 1.4$

Figure 5 Particle Trajectories Through the Solution Region

Figure 6 Particle Trajectories as a Function of Particle Radius

Figure 7 Particle Trajectories as a Function of Particle Mass Density

Figure 8 Tangential Variation of Particle-To-Gas Velocity Ratio with Particle Radius as a Parameter, $\rho_p = 1$ gm/cc

Figure 9 Tangential Variation of Particle-To-Gas Velocity Ratio with Particle Mass Density as a Parameter, r = 0.25 micron

Figure 10 Tangential Variation of Angular Deviation with Radius as a Parameter, $\rho_p = 1$ gm/cc

Figure 11 Tangential Variation of Angular Deviation with Particle Mass Density as a Parameter, r = 0.25 micron

Figure 12 Contours of Constant Particle-To-Gas Velocity Ratio, $\rho_p = 1$ gm/cc

Figure 13 Contours of Constant Angular Deviation, $\rho_p = 1$ gm/cc

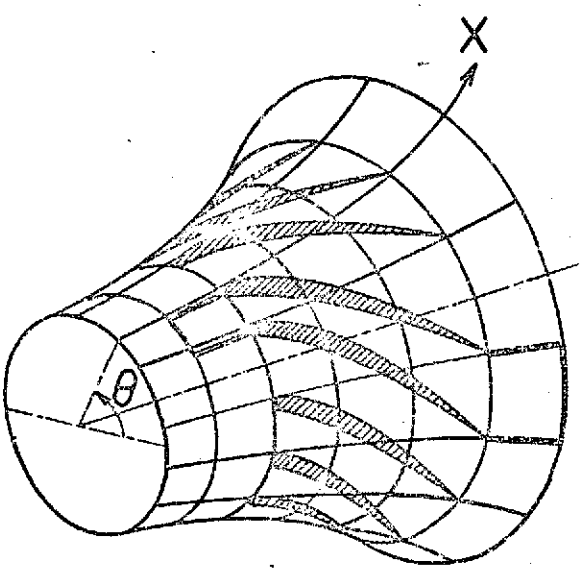

FIGURE 1 BLADE-TO-BLADE SOLUTION REGION

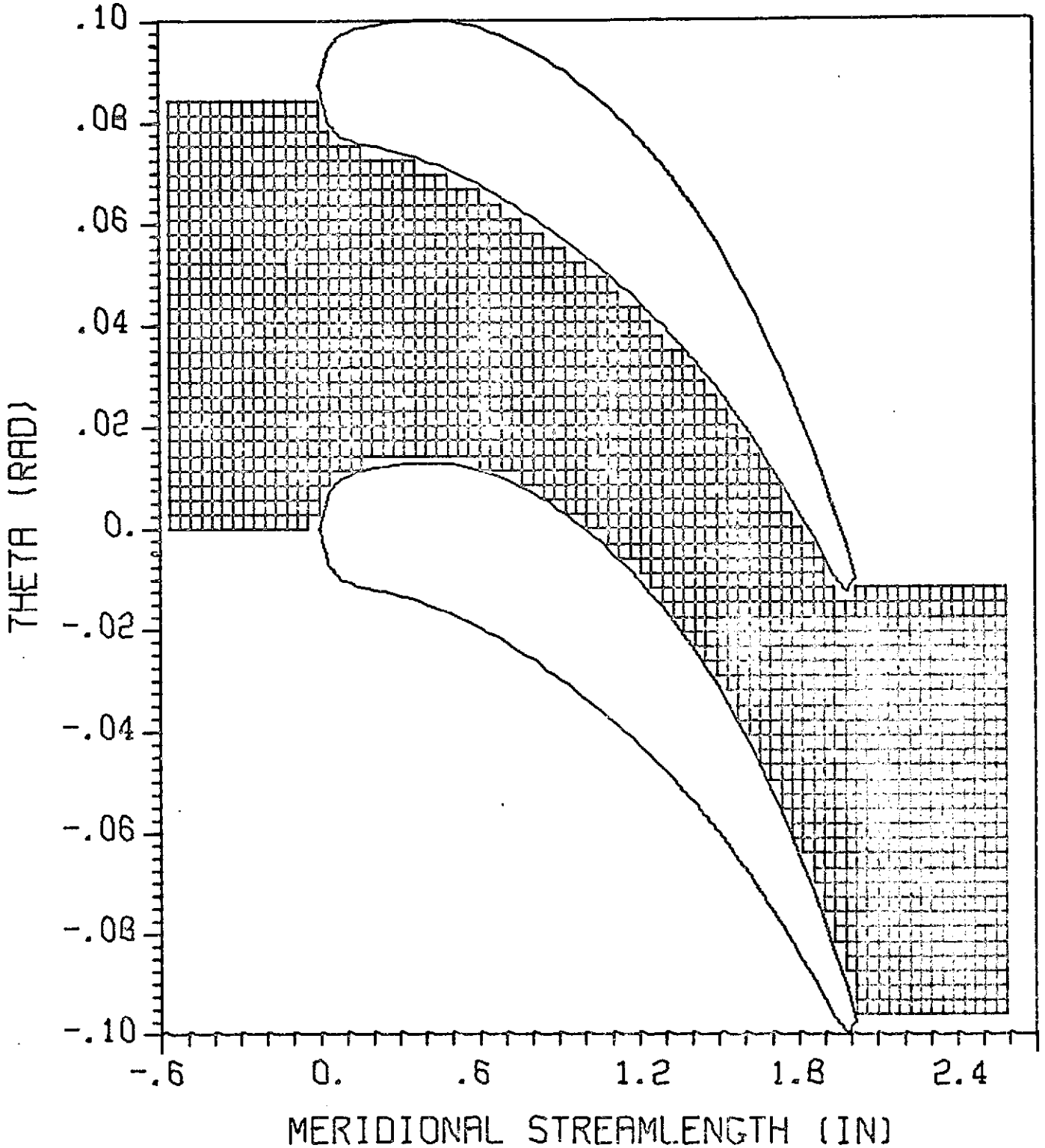

FIGURE 2 BLADE-TO-BLADE SOLUTION REGION

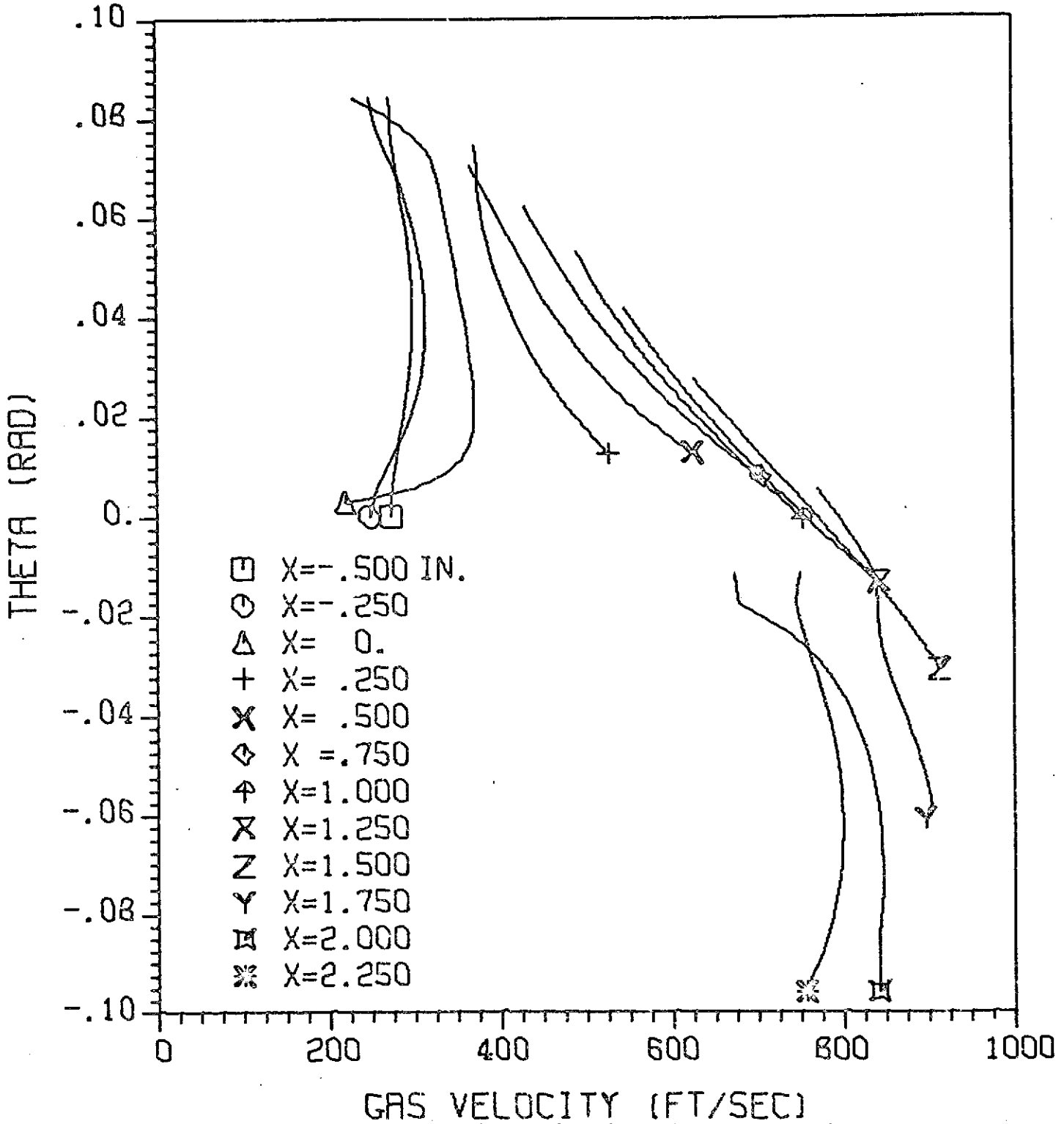

FIGURE 3 Gas Flow Velocity Profiles Across Stream Channel, $\dot{m} = 6.68 \times 10^{-3}$ lb/sec, $\rho_g = 7.403 \times 10^{-2}$ lb/ft^3, T = 523.7 R, $\gamma = 1.4$

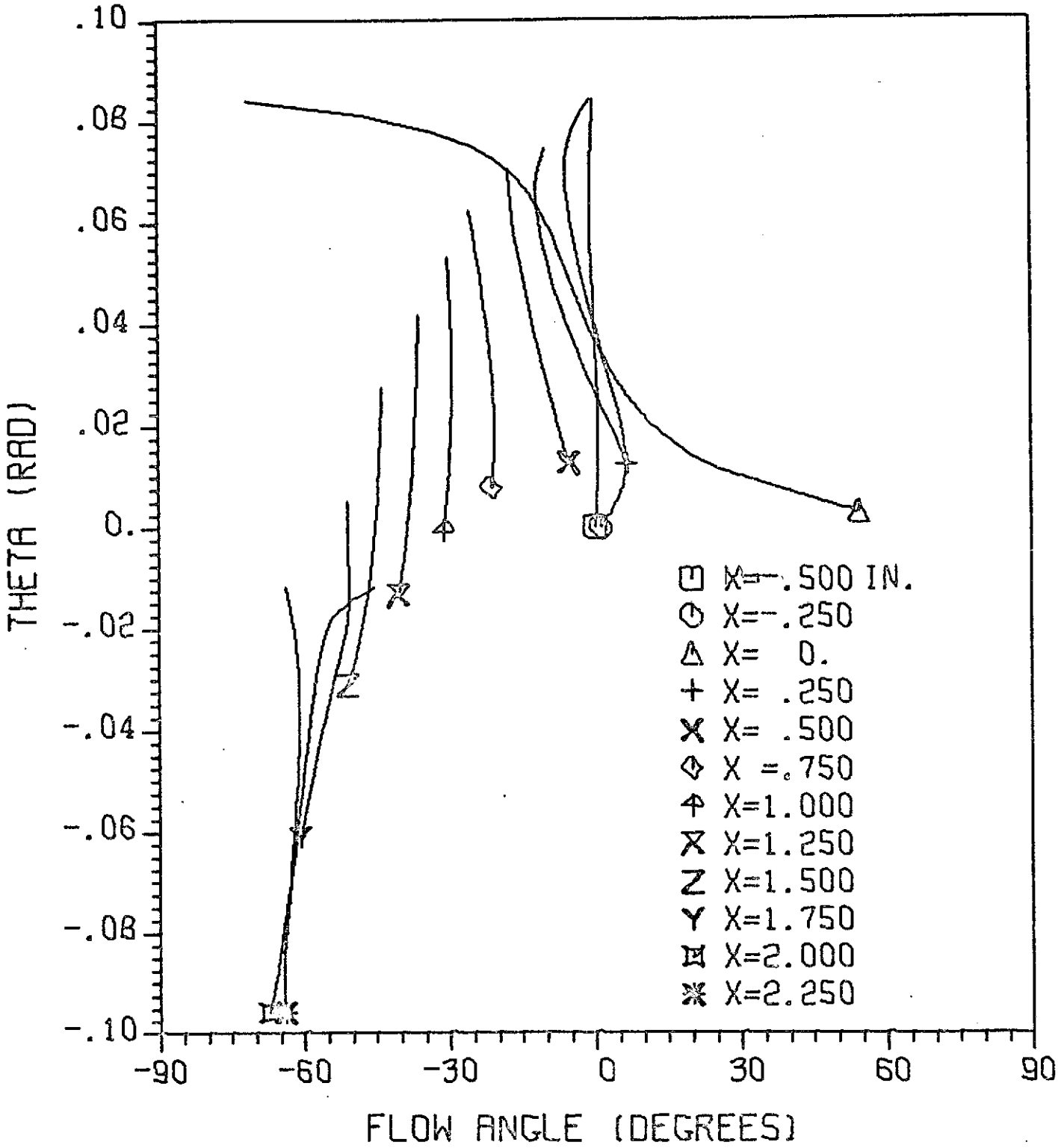

FIGURE 4 Gas Flow Angle Profiles Across Stream Channel, $\dot{m} = 6.68 \times 10^{-3}$ lb/sec, $\rho_g = 7.403 \times 10^{-2}$ lb/ft^3, T = 523.7 R, $\gamma = 1.4$

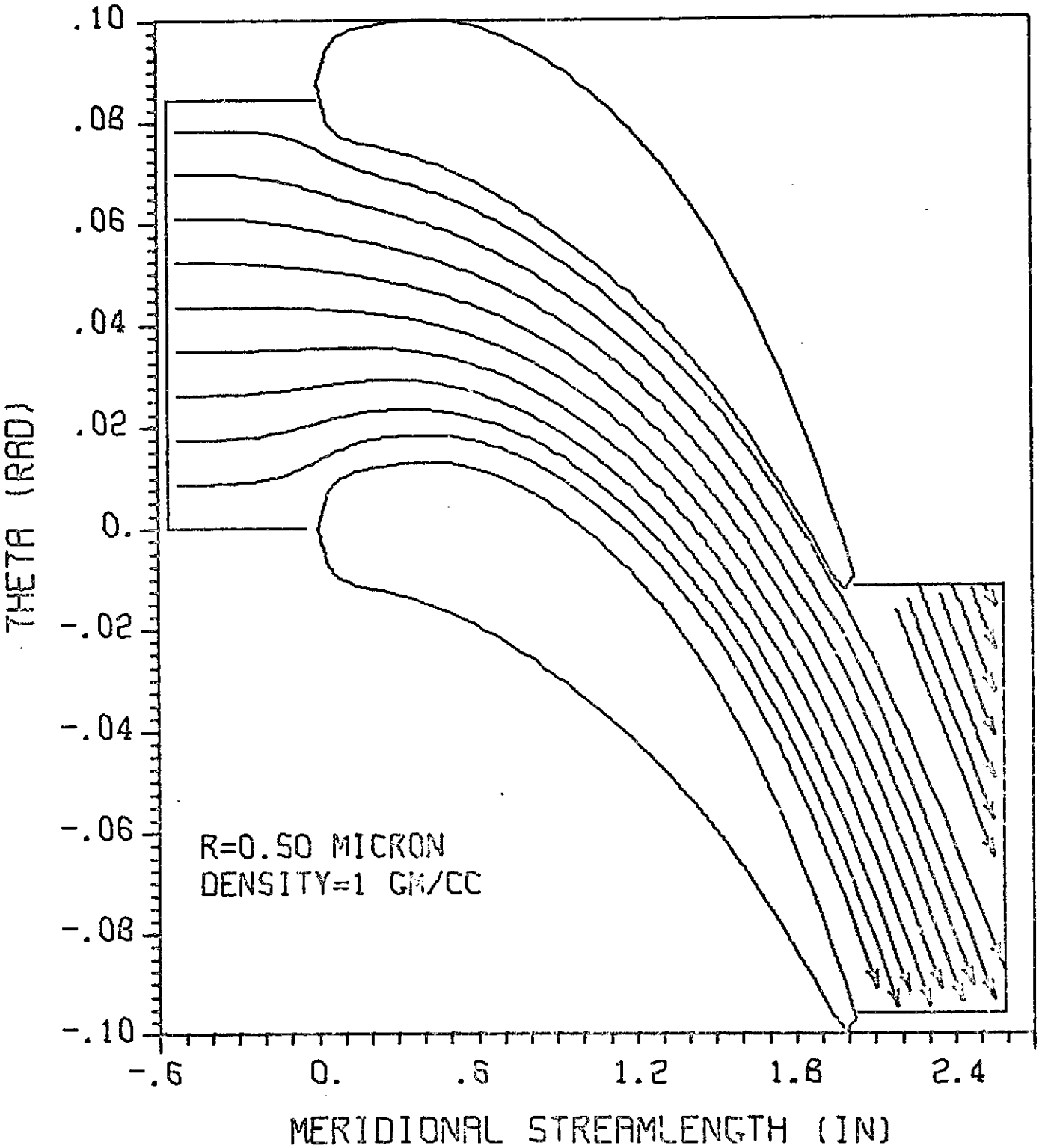

FIGURE 5 PARTICLE TRAJECTORIES THROUGH THE SOLUTION REGION

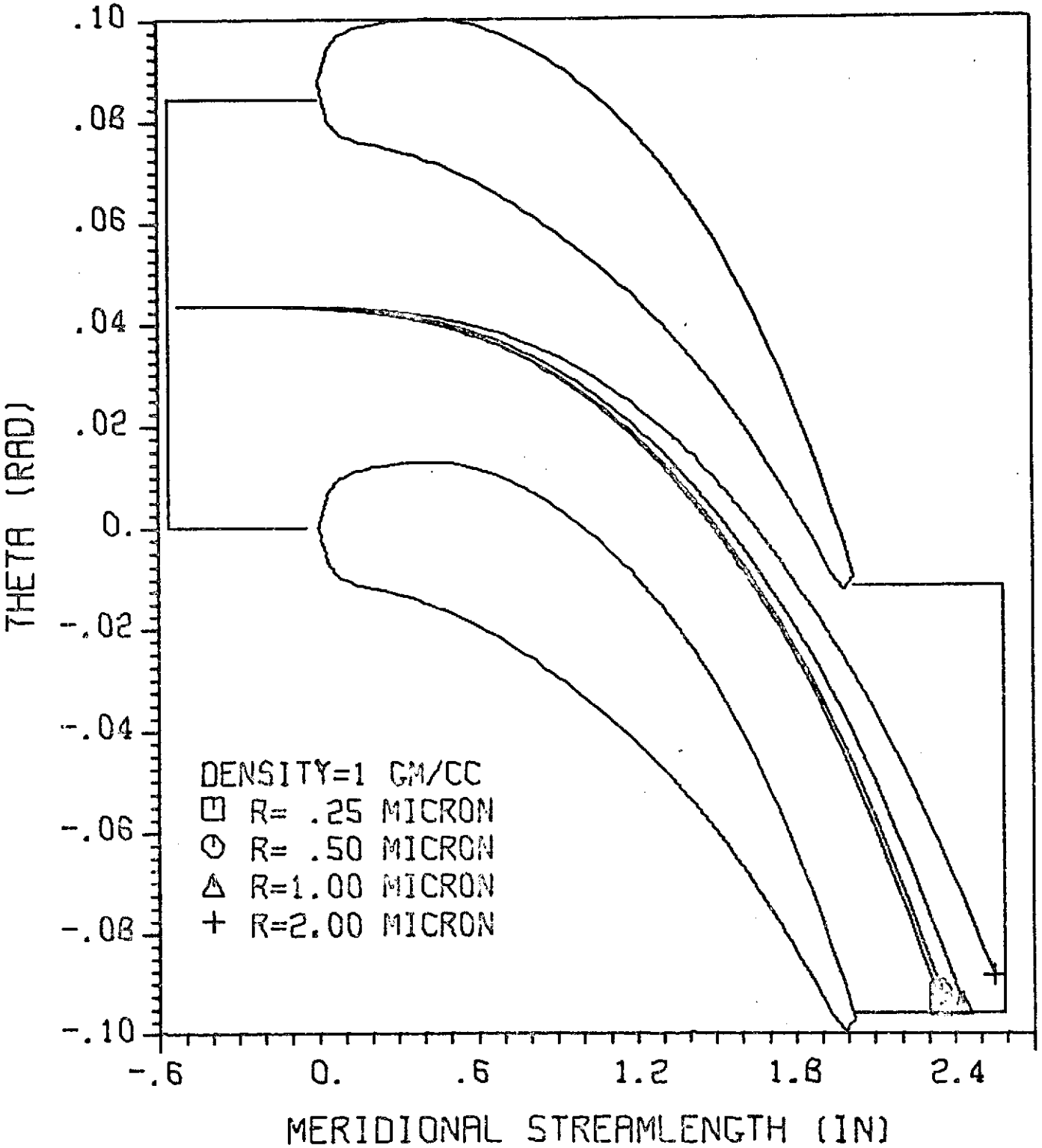

FIGURE 6 PARTICLE TRAJECTORIES AS A FUNCTION OF PARTICLE RADIUS

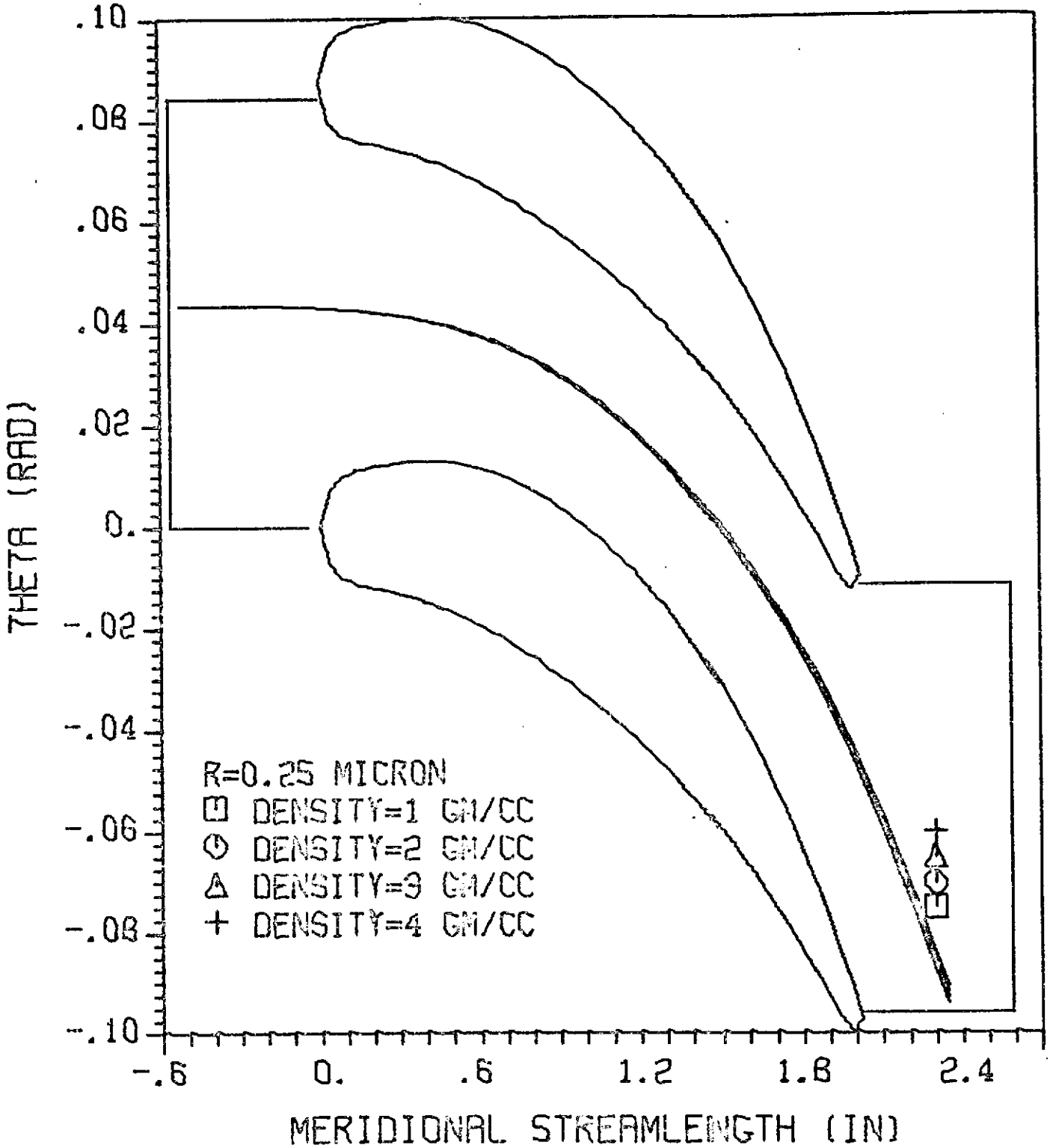

FIGURE 7 PARTICLE TRAJECTORIES AS A FUNCTION OF PARTICLE MASS DENSITY

FIGURE 8

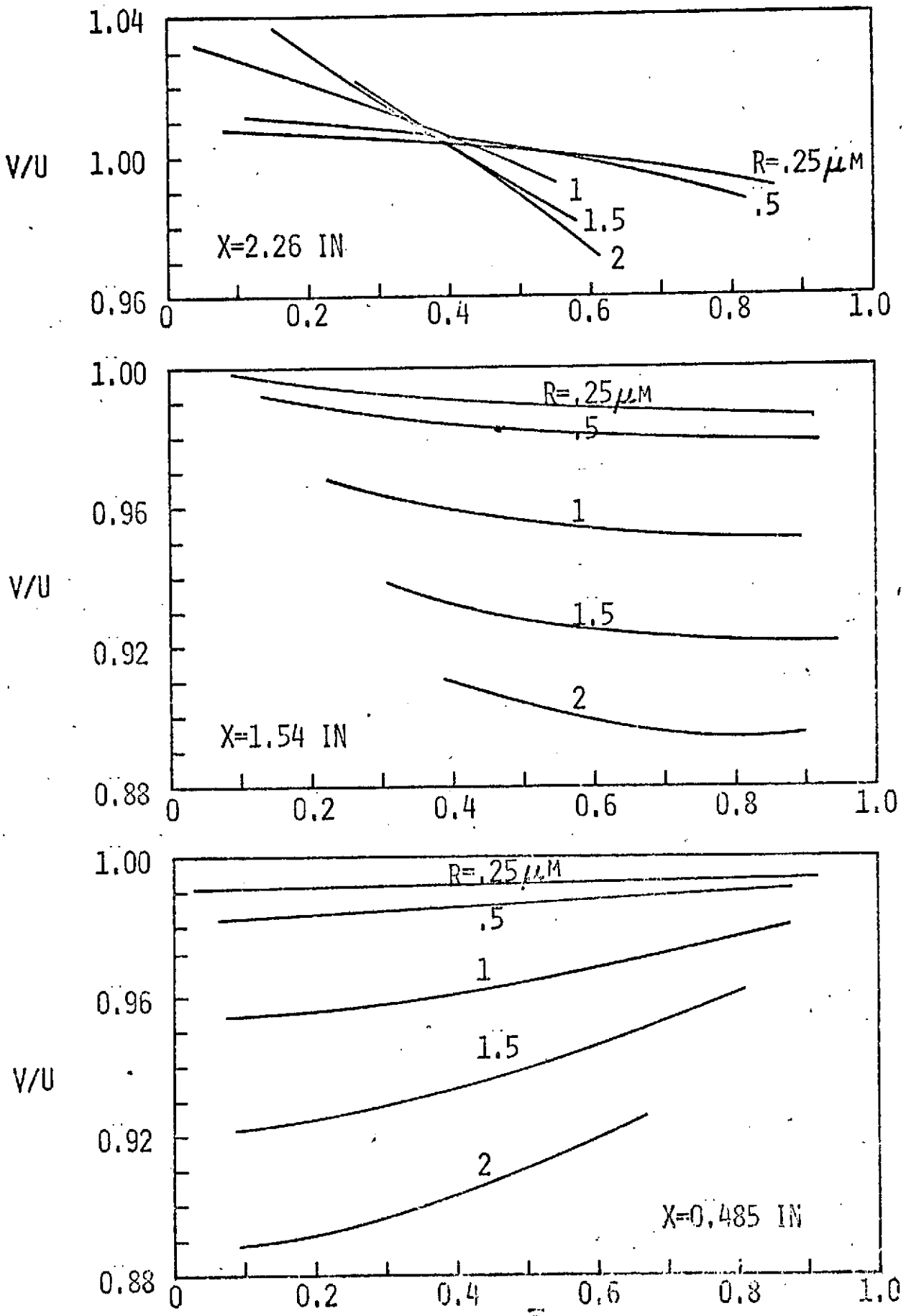
1.04
1.00
0.96
V/U
R=.25μM
.5
1
1.5
2
X=2.26 IN
0
0.2
0.4
0.6
0.8
1.0
1.00
0.96
0.92
0.88
V/U
R=.25μM
.5
1
1.5
2
X=1.54 IN
0
0.2
0.4
0.6
0.8
1.0
1.00
0.96
0.92
0.88
V/U
R=.25μM
.5
1
1.5
2
X=0.485 IN
0
0.2
0.4
0.6
0.8
1.0
θ̄

FIGURE 9

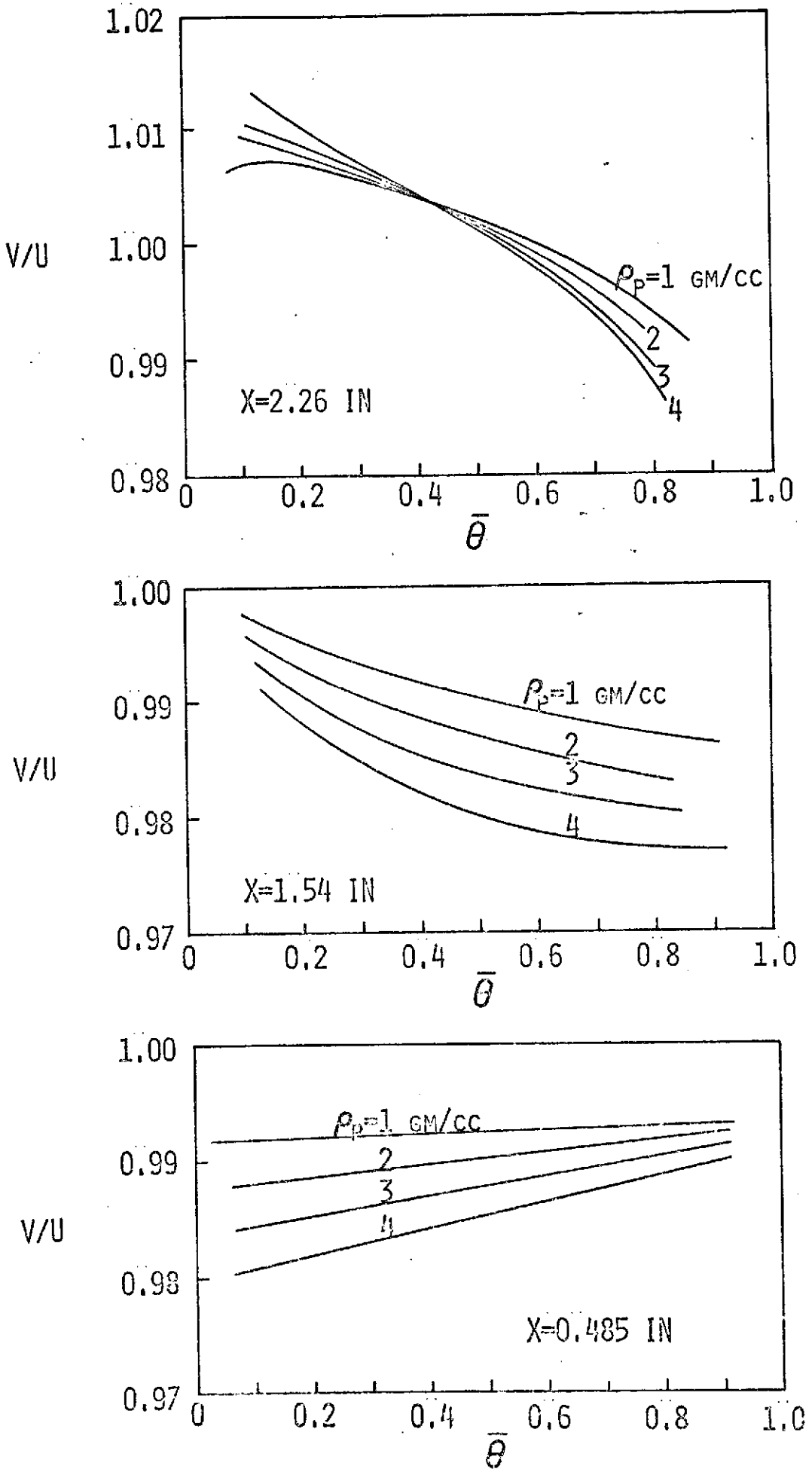
1.02
1.01
1.00
0.99
0.98
V/U
ρ_p=1 GM/CC
2
3
4
X=2.26 IN
0
0.2
0.4
0.6
0.8
1.0
$\bar{\theta}$
1.00
0.99
0.98
0.97
V/U
ρ_p=1 GM/CC
2
3
4
X=1.54 IN
0
0.2
0.4
0.6
0.8
1.0
$\bar{\theta}$
1.00
0.99
0.98
0.97
V/U
ρ_p=1 GM/CC
2
3
4
X=0.485 IN
0
0.2
0.4
0.6
0.8
1.0
$\bar{\theta}$

FIGURE 10

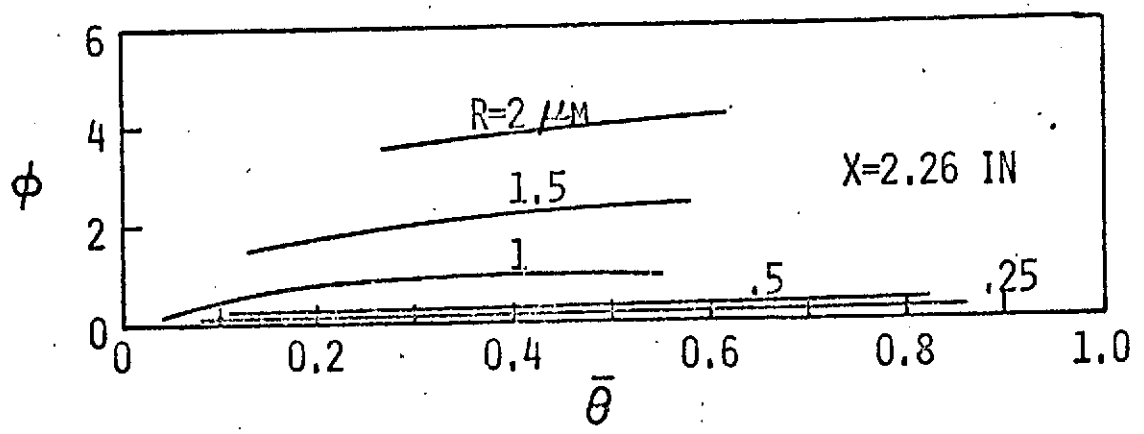
6
4
2
0
ϕ
R=2 μM
1.5
1
.5
.25
X=2.26 IN
0
0.2
0.4
0.6
0.8
1.0
$\bar{\theta}$

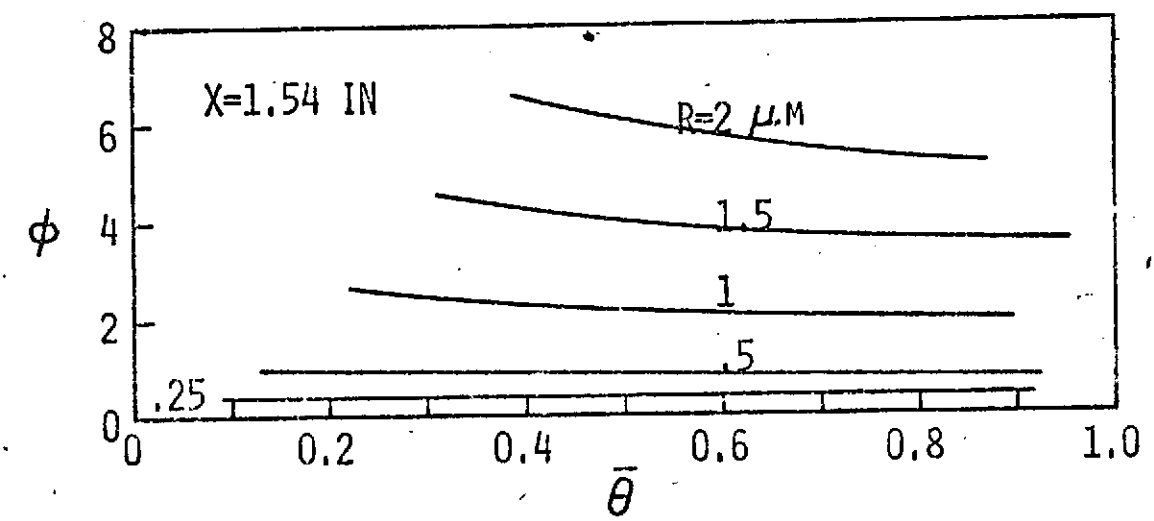
8
6
4
2
0
ϕ
X=1.54 IN
R=2 μM
1.5
1
.5
.25
0
0.2
0.4
0.6
0.8
1.0
$\bar{\theta}$

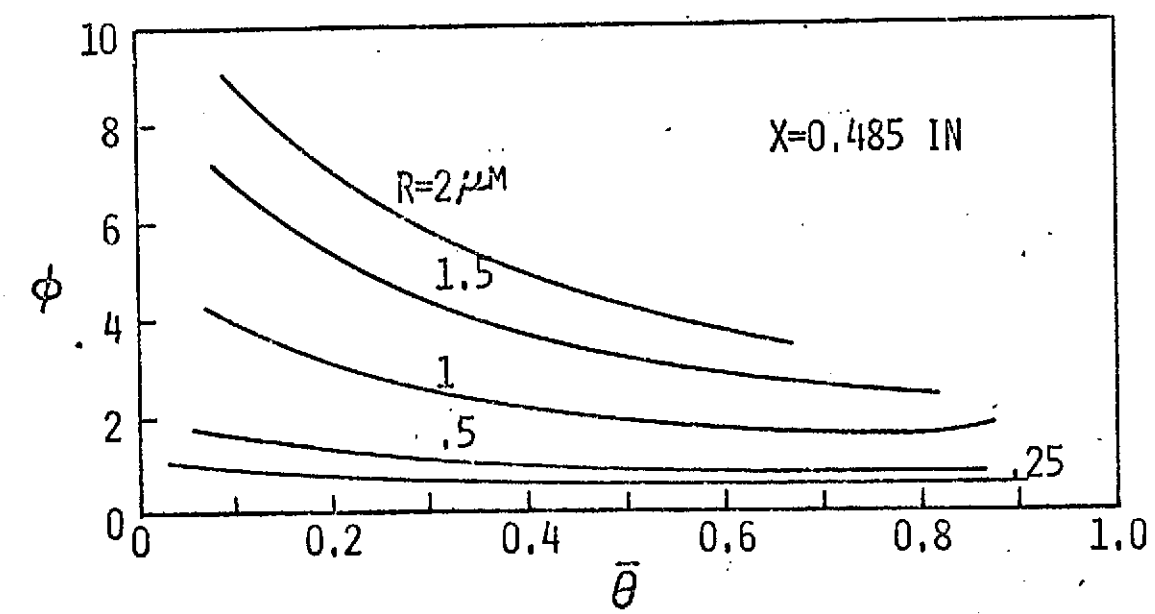
10
8
6
4
2
0
ϕ
X=0.485 IN
R=2 μM
1.5
1
.5
.25
0
0.2
0.4
0.6
0.8
1.0
$\bar{\theta}$

FIGURE 11

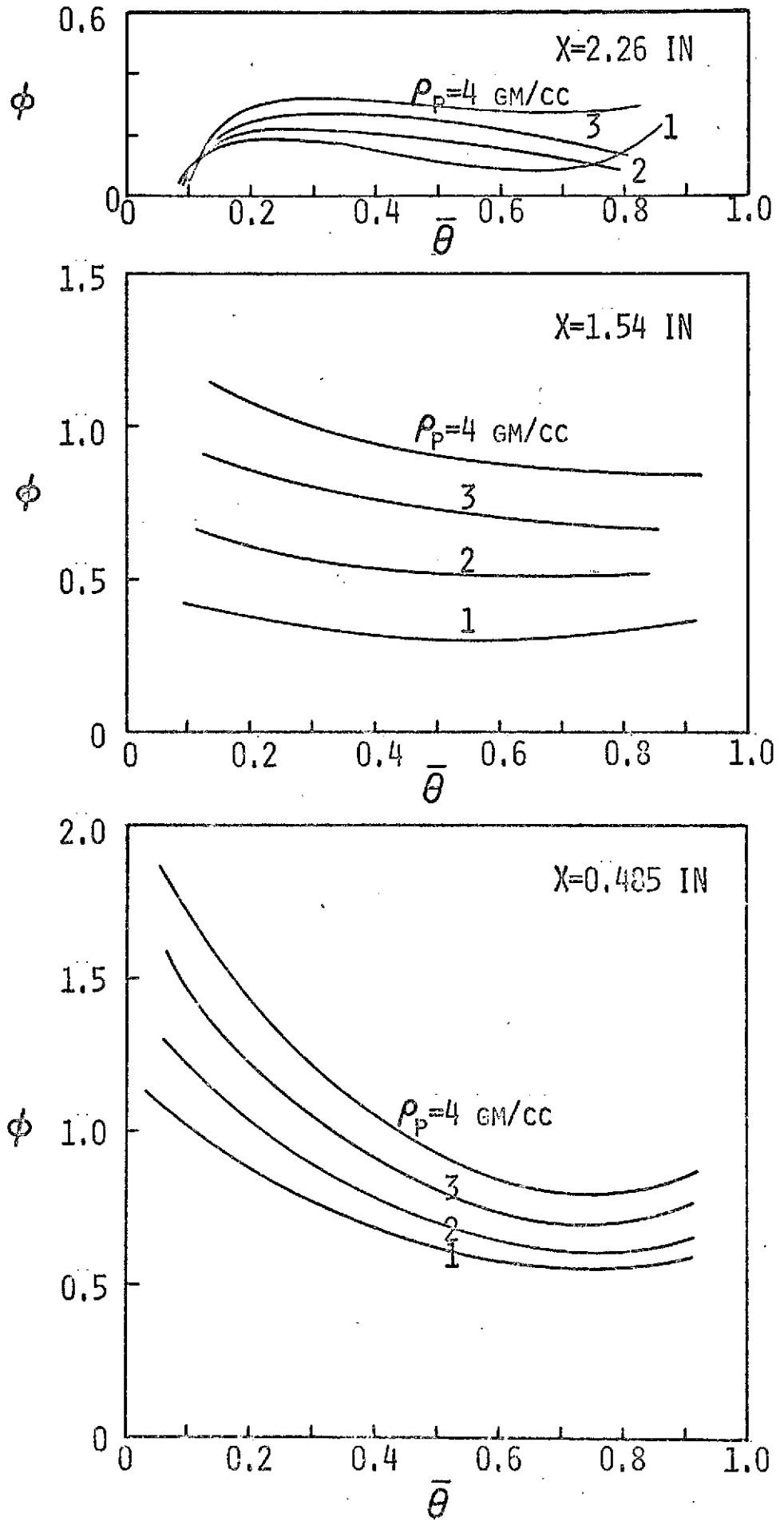
X=2.26 IN
ρ_p=4 GM/CC
3
1
2
ϕ
$\bar{\theta}$
0.6
0
0.2
0.4
0.6
0.8
1.0
X=1.54 IN
ρ_p=4 GM/CC
3
2
1
1.5
1.0
0.5
X=0.485 IN
ρ_p=4 GM/CC
3
2
1
2.0

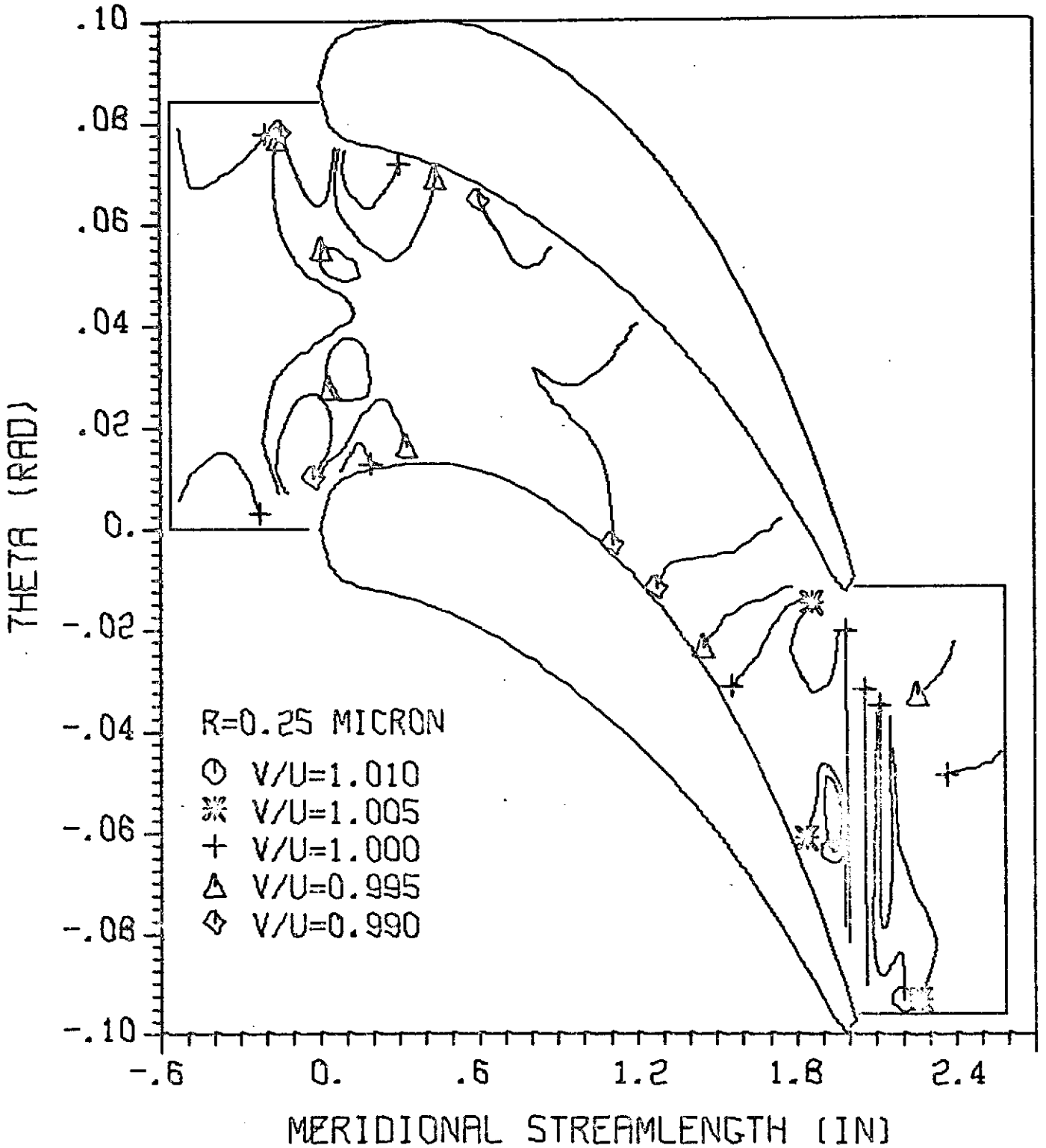

FIGURE 12A CONTOURS OF CONSTANT PARTICLE-TO-GAS VELOCITY RATIO,

ρ_p = 1 gm/cc

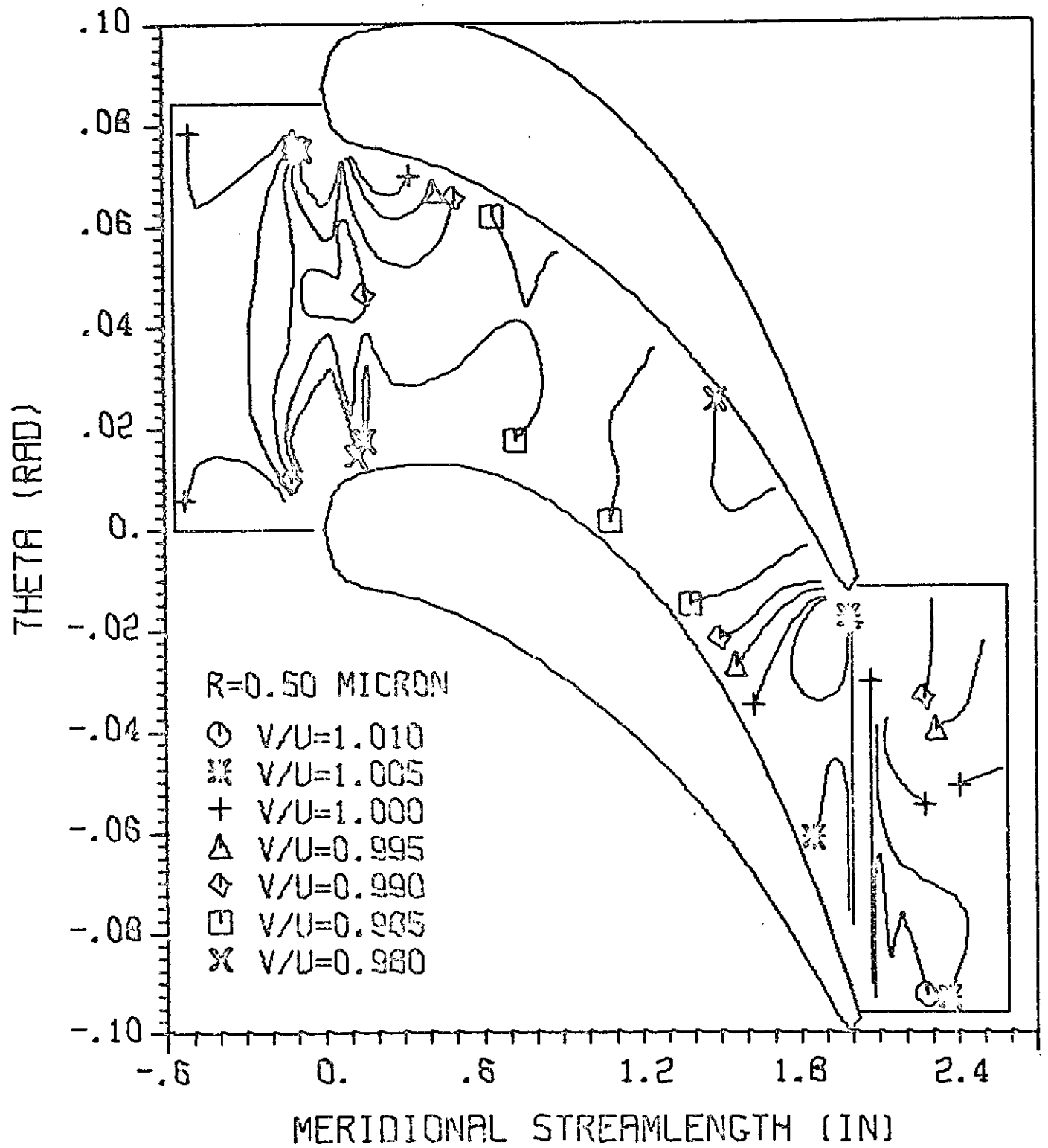

FIGURE 12B CONTOURS OF CONSTANT PARTICLE-TO-GAS VELOCITY RATIO, ρ_p = 1 gm/cc

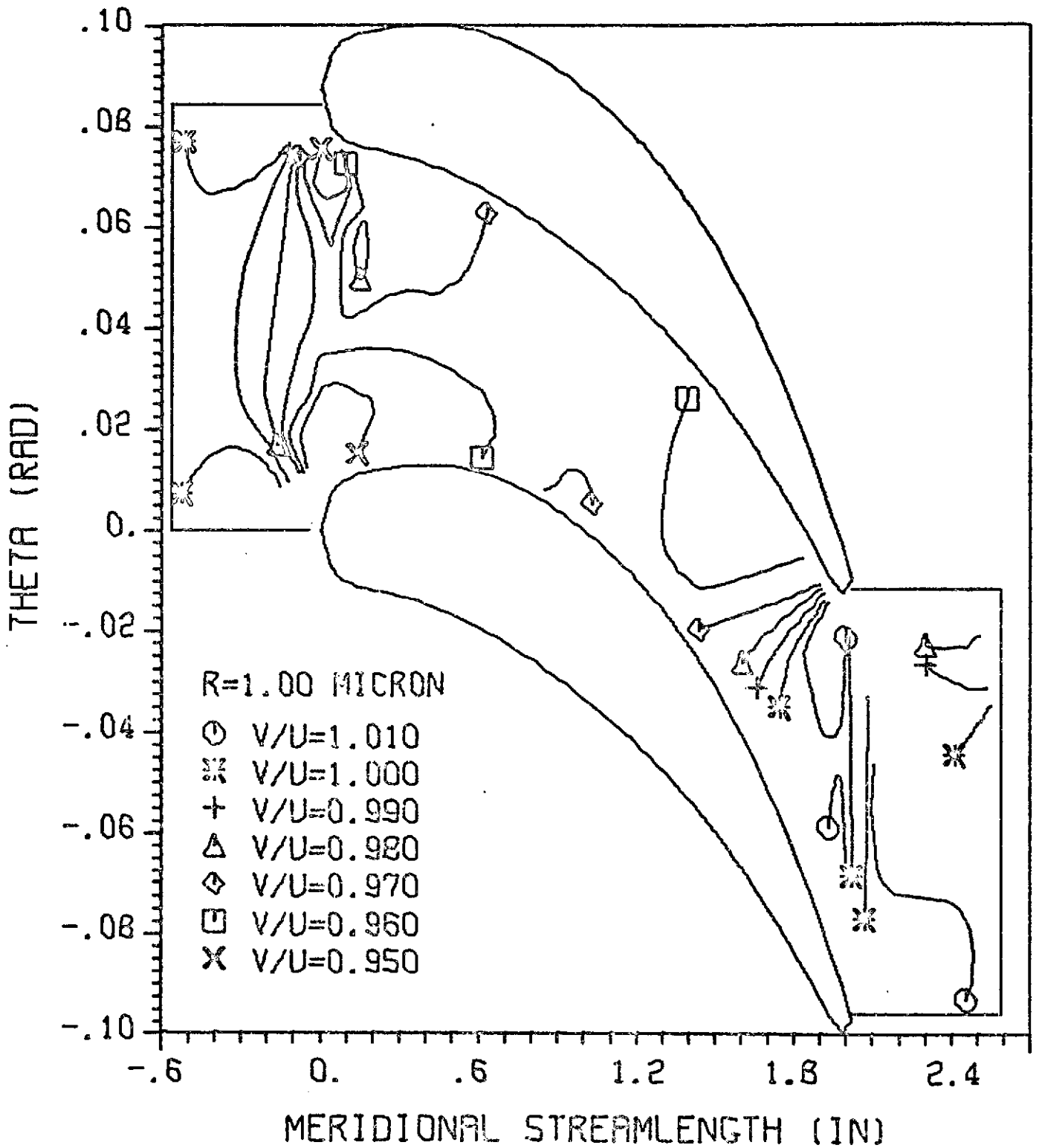

FIGURE 12c CONTOURS OF CONSTANT PARTICLE-TO-GAS VELOCITY RATIO, ρ_p = 1 gm/cc

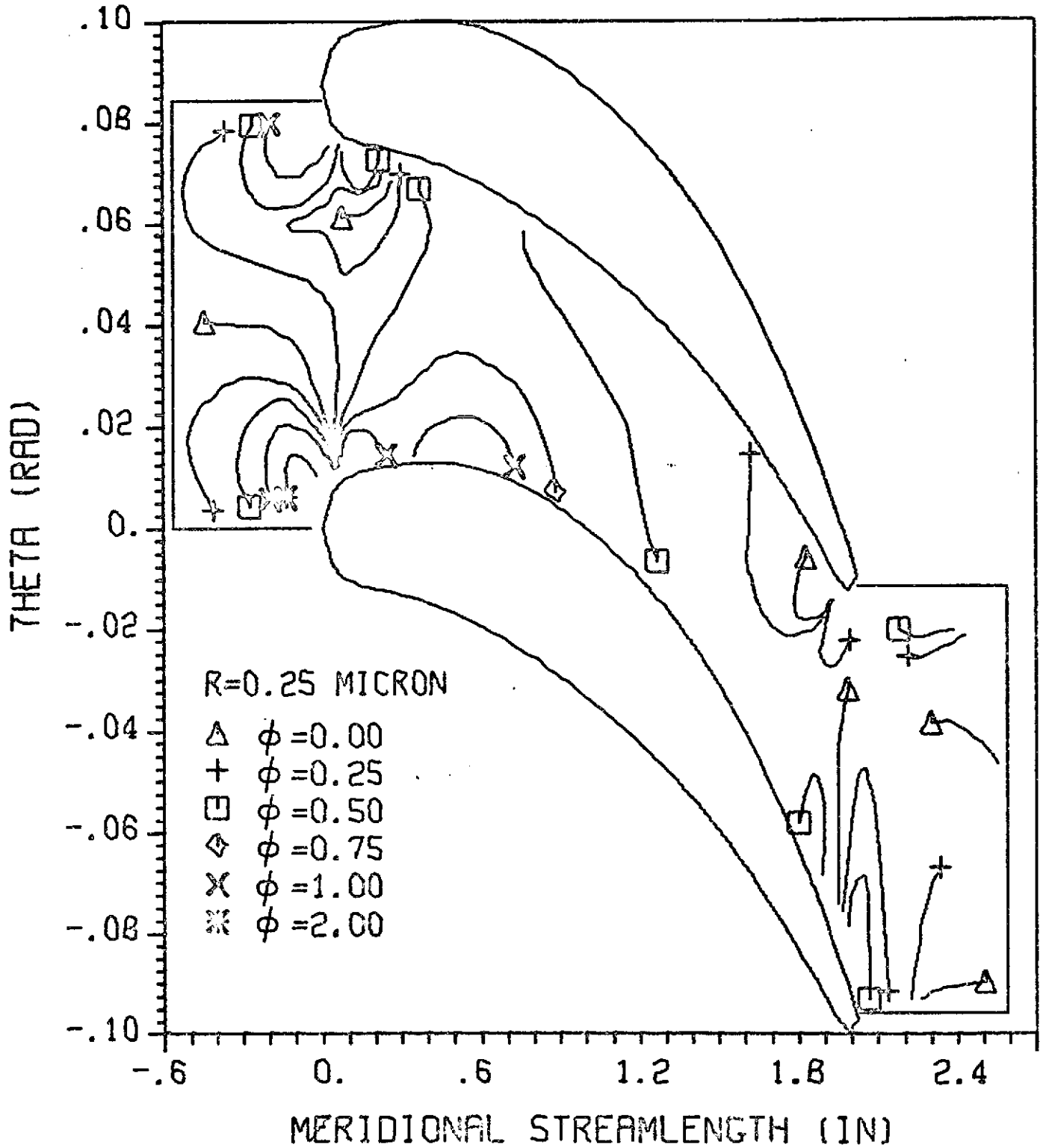

FIGURE 13A CONTOURS OF CONSTANT ANGULAR DEVIATION,

ρ_p = 1 gm/cc

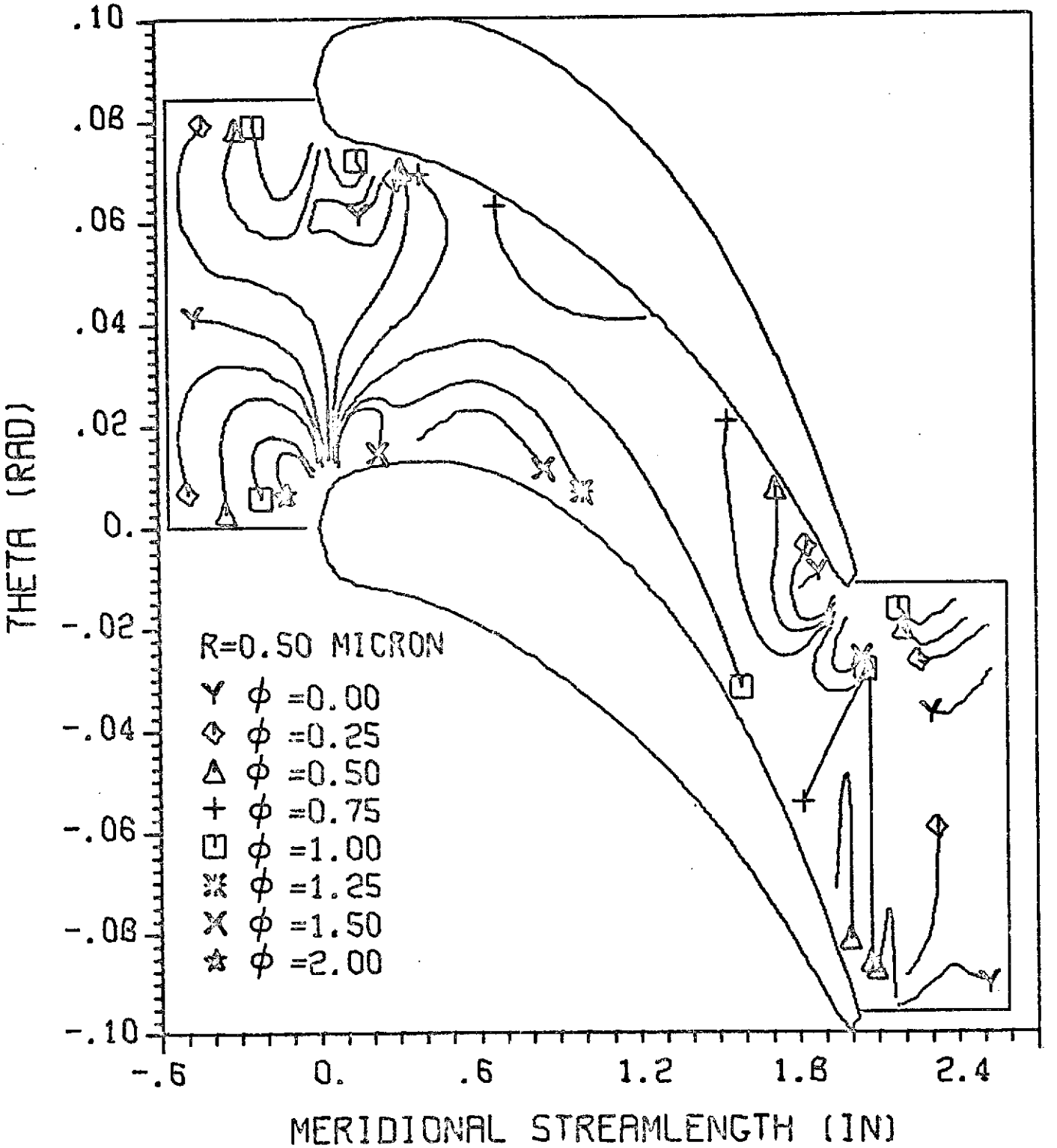

FIGURE 13B CONTOURS OF CONSTANT ANGULAR DEVIATION,

ρ_p = 1 gm/cc

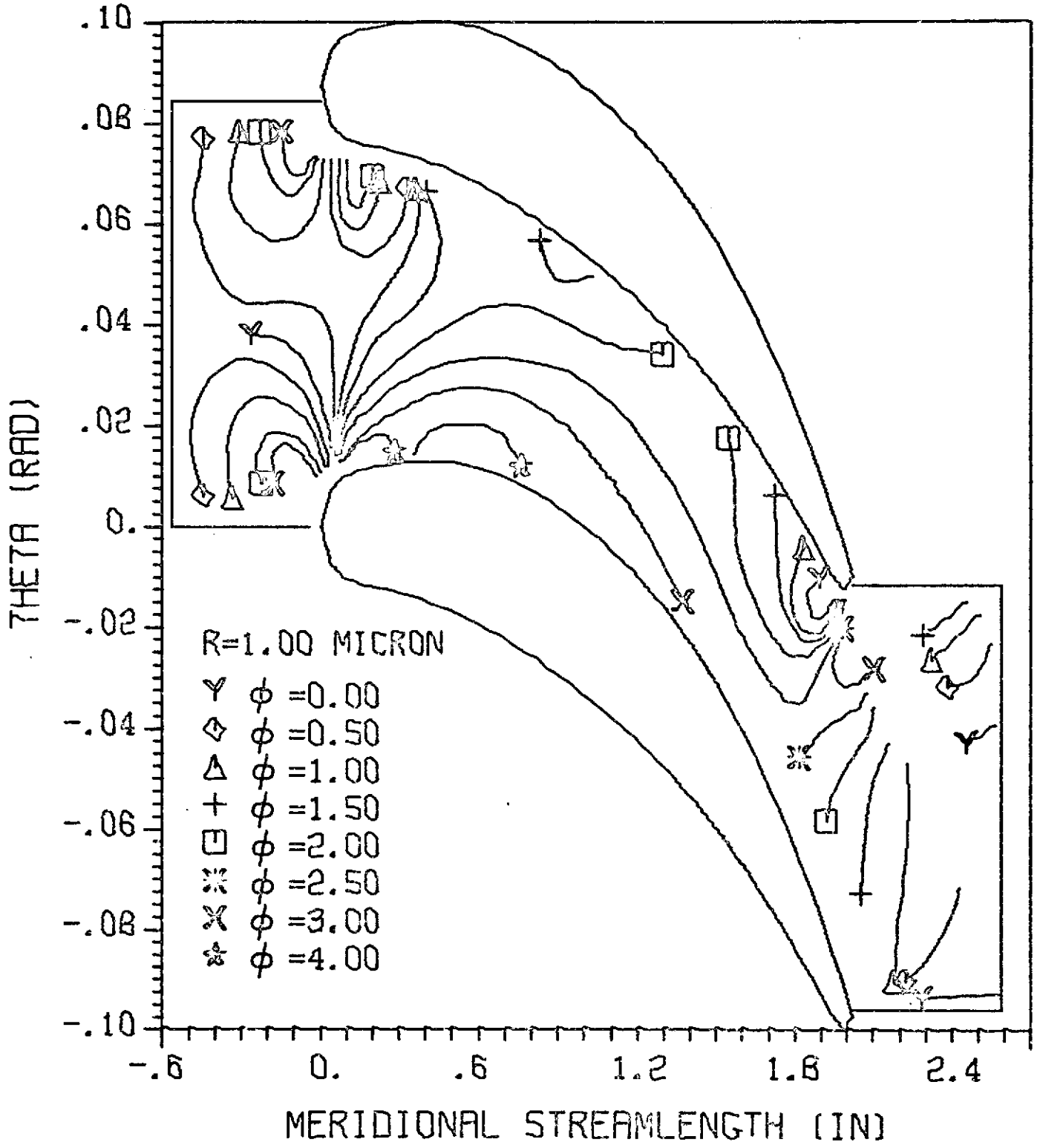

FIGURE 13c CONTOURS OF CONSTANT ANGULAR DEVIATION,

ρ_p = 1 gm/cc

Do not Print

REPORT DISTRIBUTION LIST FOR NASA CR-134543

Recipient	Address
Dr. Richard G. Seasholtz (3)	NASA Lewis Research Center 21000 Brookpark Road Cleveland, OH 44135 Mail Stop 77-1
Mr. Melvin J. Hartmann (1)	NASA Lewis Research Center 21000 Brookpark Road Cleveland, OH 44135 Mail Stop 5-9
Mr. Theodore Katsanis (1)	NASA Lewis Research Center 21000 Brookpark Road Cleveland, OH 44135 Mail Stop 77-2
Patent Counsel (1)	NASA Lewis Research Center 21000 Brookpark Road Cleveland, OH 44135 Attention: Norman T. Musial
Lewis Library (2)	NASA Lewis Research Center 21000 Brookpark Road Cleveland, OH 44135 Attention: Library
Lewis Technical Information Division (1)	NASA Lewis Research Center 21000 Brookpark Road Cleveland, OH 44135 Attention: Report Control Office
NASA Headquarters Technical information abstracting and dissemenation facility (6)	NASA Scientific and Technical Information Facility Box 5700 Bethesda, MD 20014 Attention: NASA Representative
Mr. Wayne Park (1)	NASA Lewis Research Center 21000 Brookpark Road Cleveland, OH 44135 Mail Stop 500-312

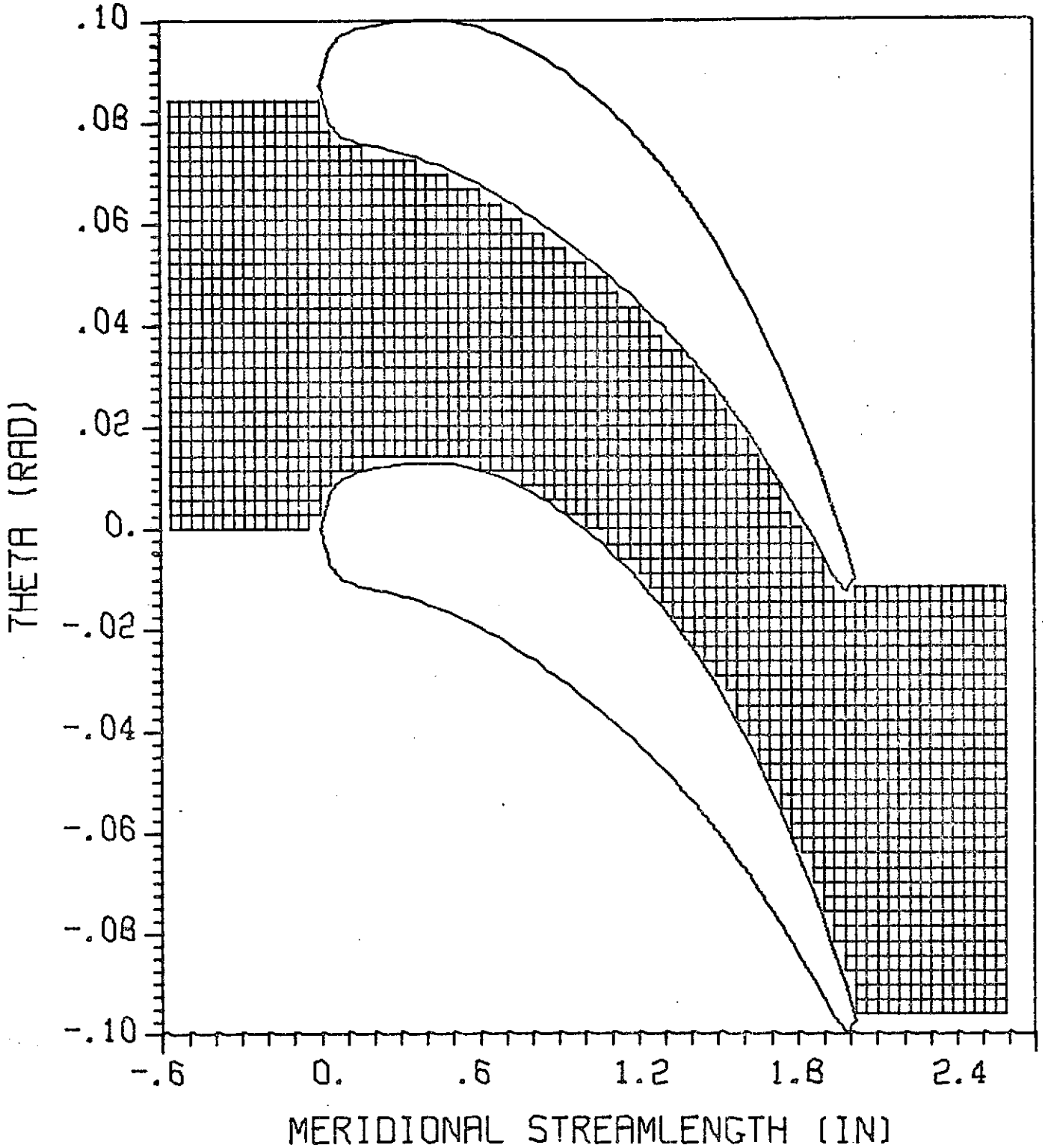

FIGURE 2 BLADE-TO-BLADE SOLUTION REGION

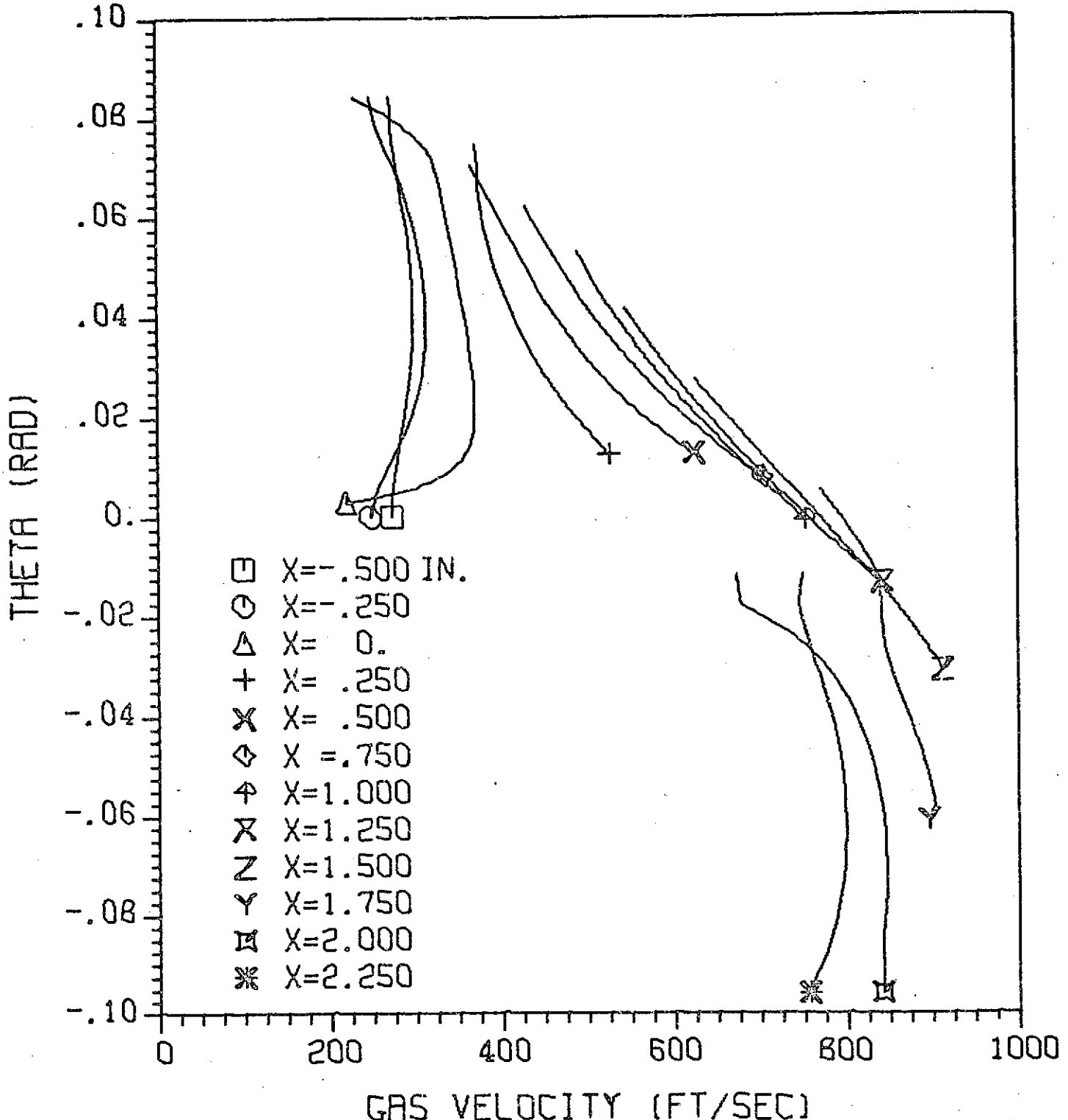

FIGURE 3 Gas Flow Velocity Profiles Across Stream Channel, $\dot{m} = 6.68 \times 10^{-3}$ lb/sec, $\rho_g = 7.403 \times 10^{-2}$ lb/ft^3, T = 523.7 R, $\gamma = 1.4$

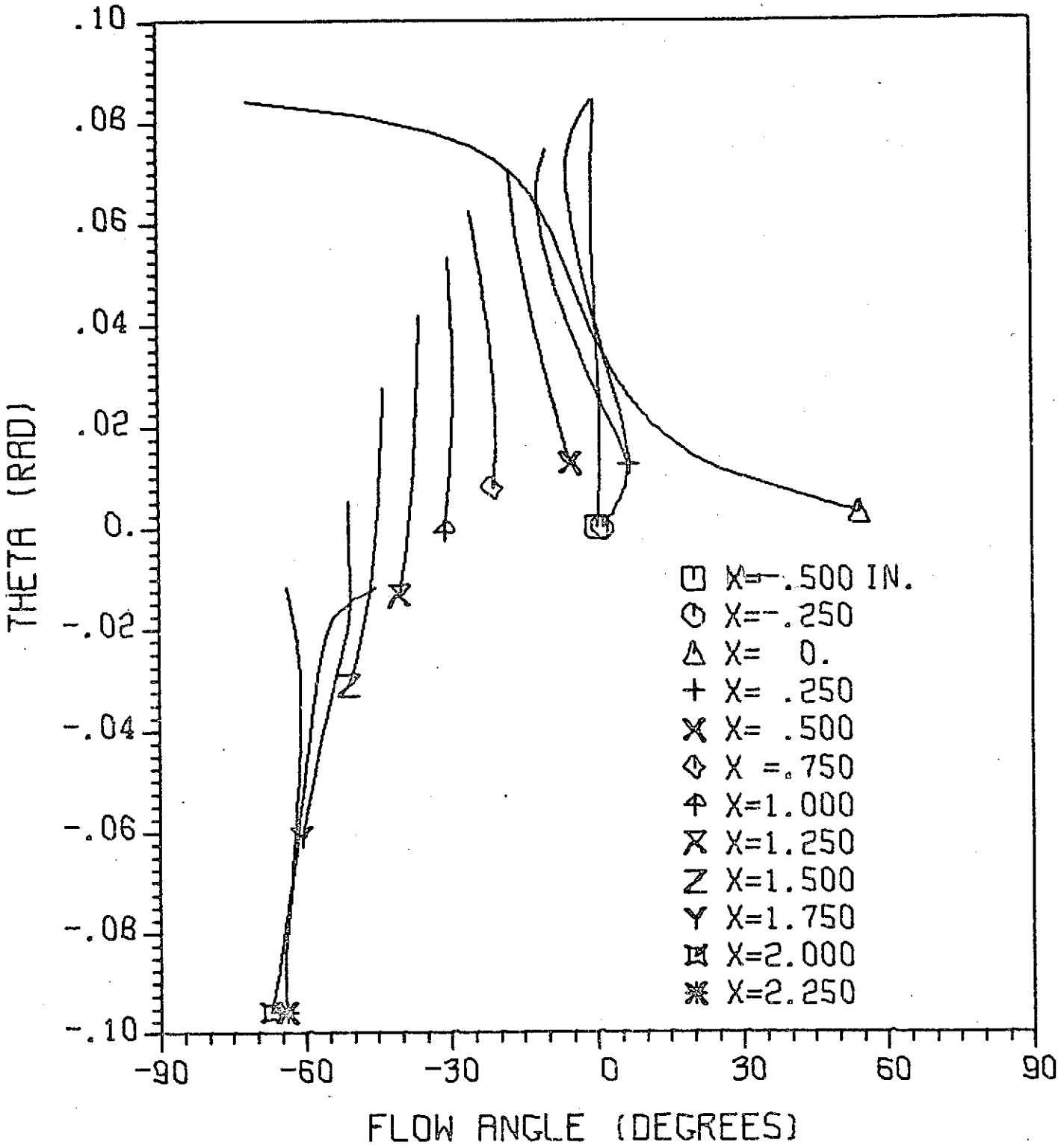

FIGURE 4 Gas Flow Angle Profiles Across Stream Channel, $\dot{m} = 6.68 \times 10^{-3}$ lb/sec, $\rho_g = 7.403 \times 10^{-2}$ lb/ft^3, T = 523.7 R, $\gamma = 1.4$

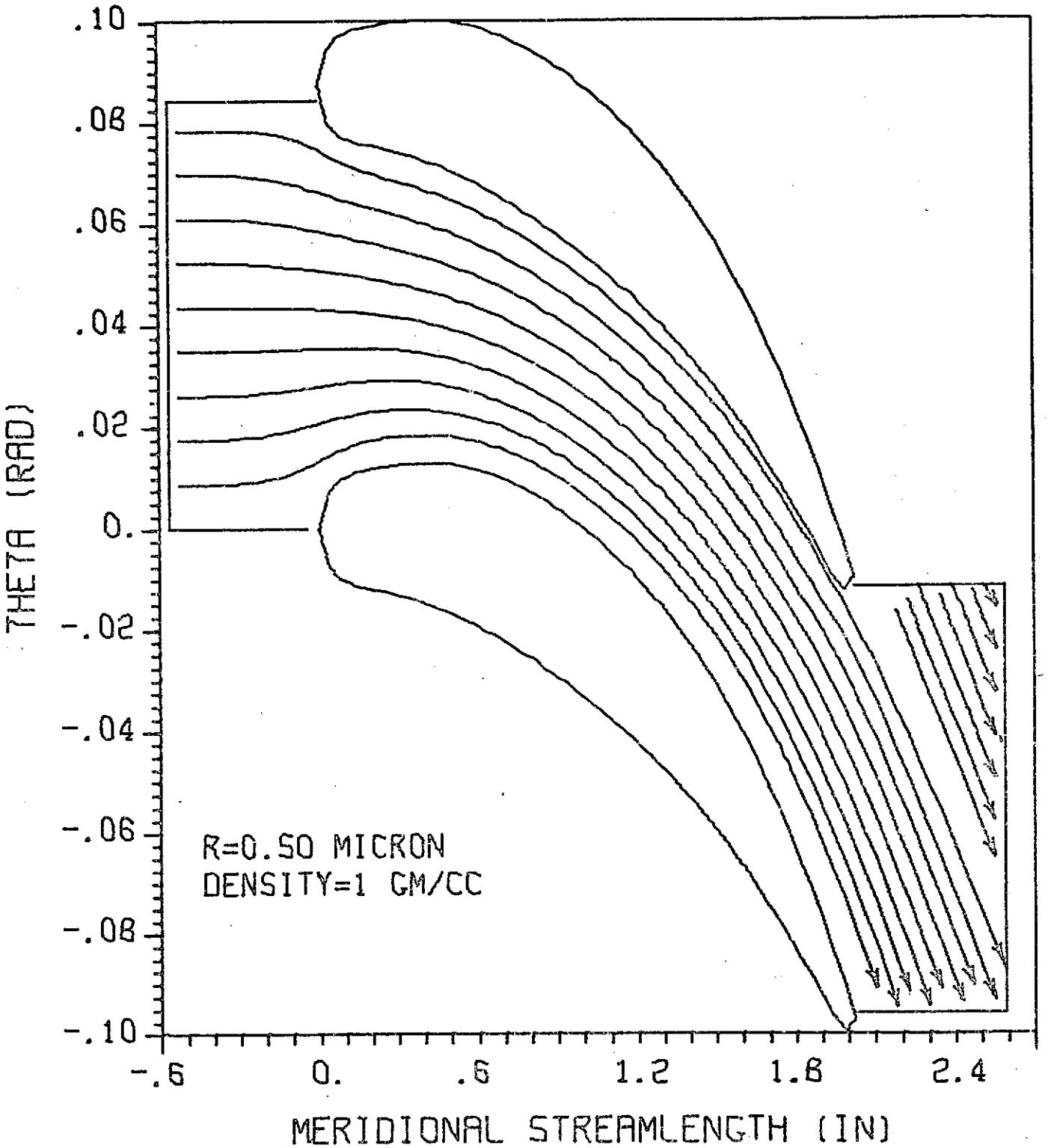

FIGURE 5 PARTICLE TRAJECTORIES THROUGH THE SOLUTION REGION

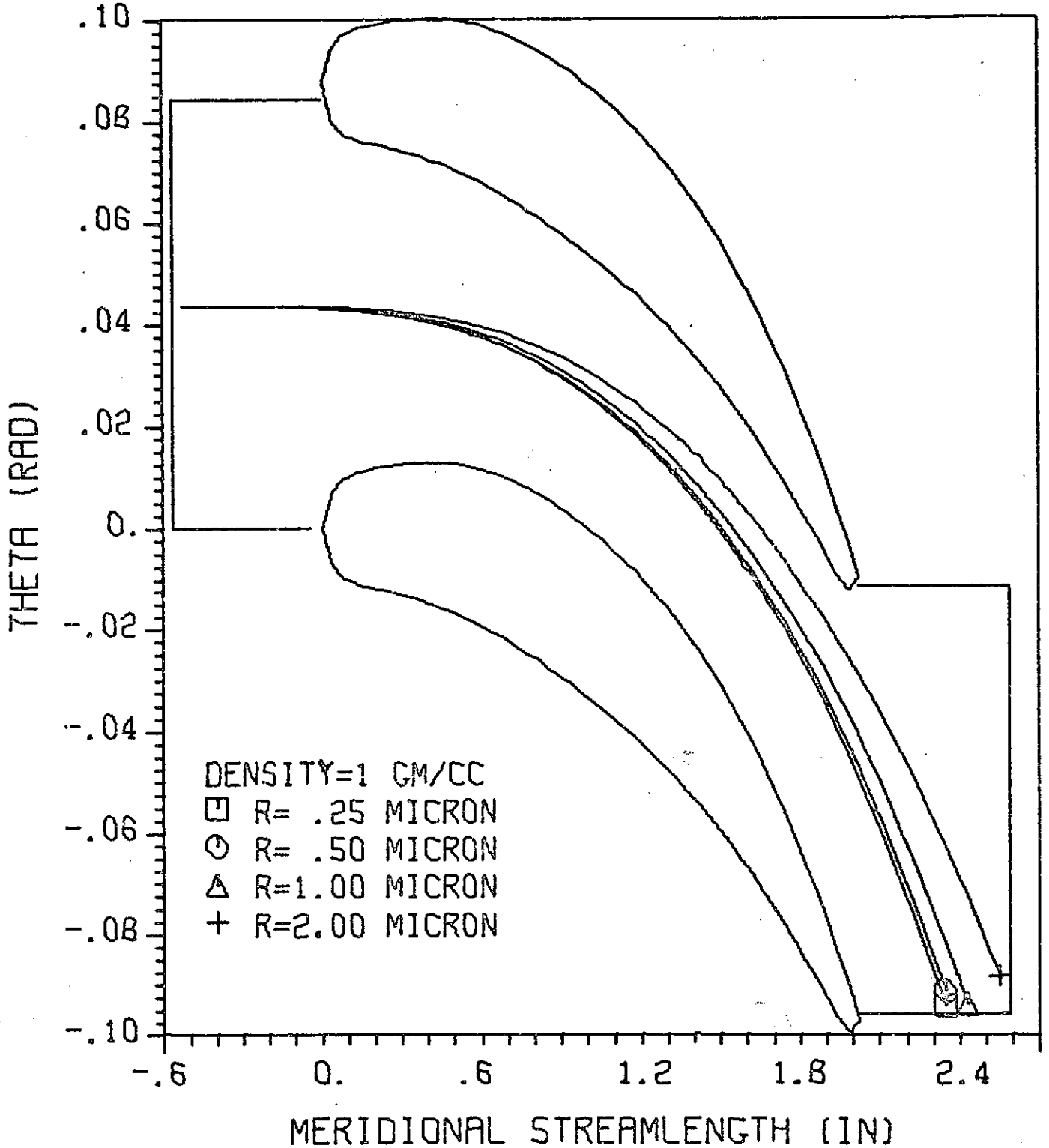

FIGURE 6 PARTICLE TRAJECTORIES AS A FUNCTION OF PARTICLE RADIUS

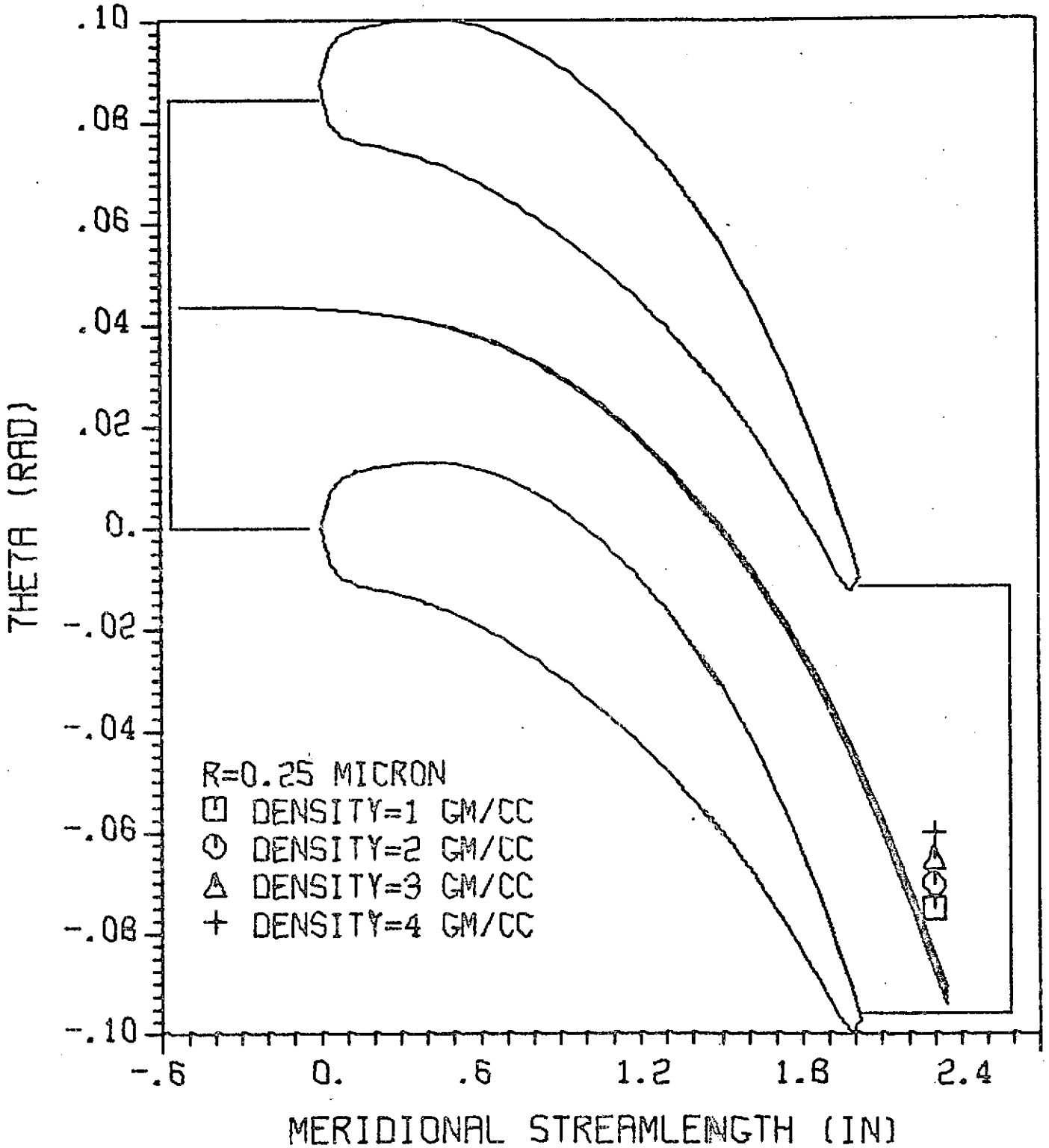

FIGURE 7 PARTICLE TRAJECTORIES AS A FUNCTION OF PARTICLE MASS DENSITY

FIGURE 8

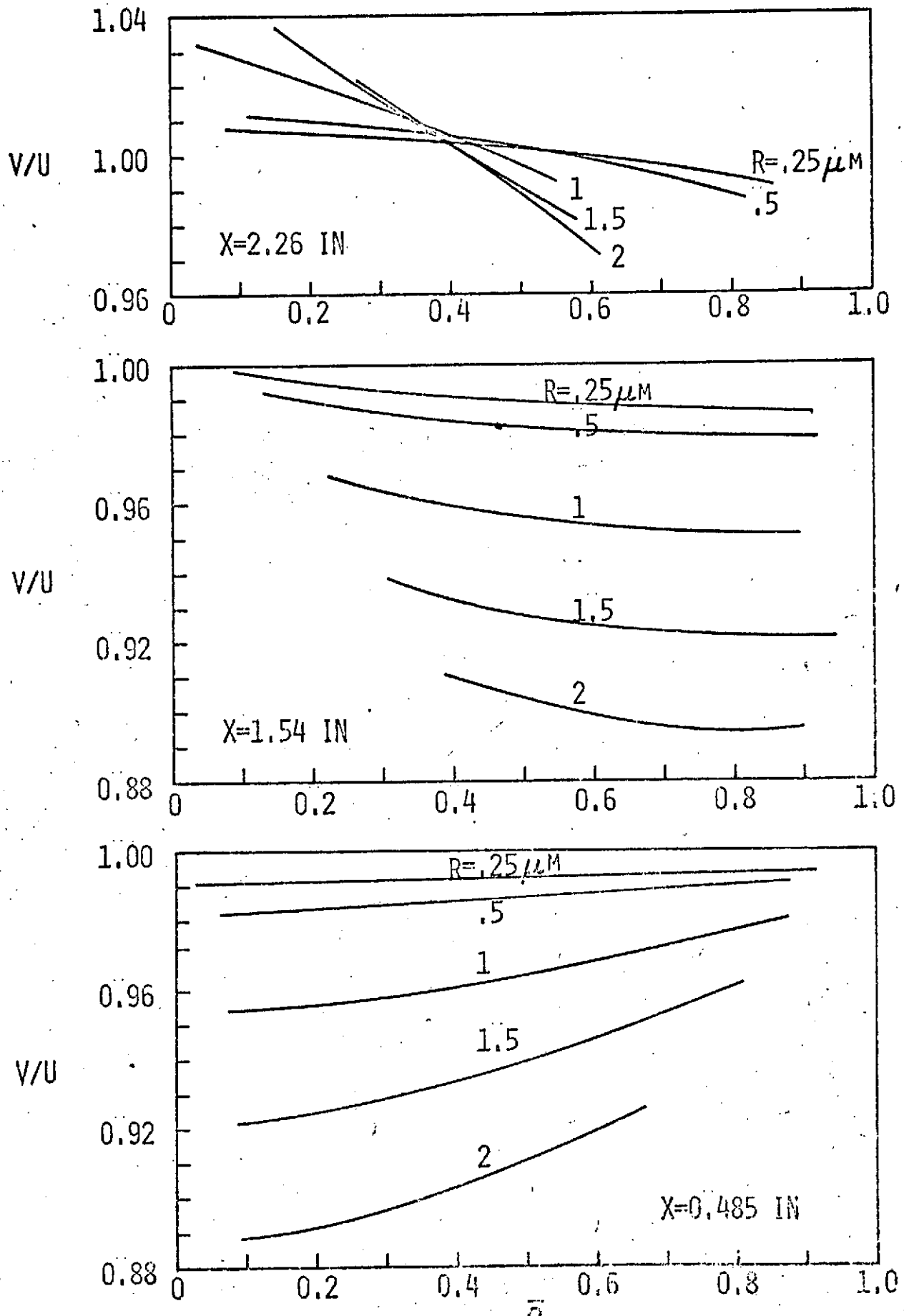
1.04
1.00
0.96
V/U
R=.25μM
.5
1
1.5
2
X=2.26 IN
0
0.2
0.4
0.6
0.8
1.0
1.00
0.96
0.92
0.88
V/U
R=.25μM
.5
1
1.5
2
X=1.54 IN
0
0.2
0.4
0.6
0.8
1.0
1.00
0.96
0.92
0.88
V/U
R=.25μM
.5
1
1.5
2
X=0.485 IN
0
0.2
0.4
0.6
0.8
1.0
θ̄

FIGURE 9

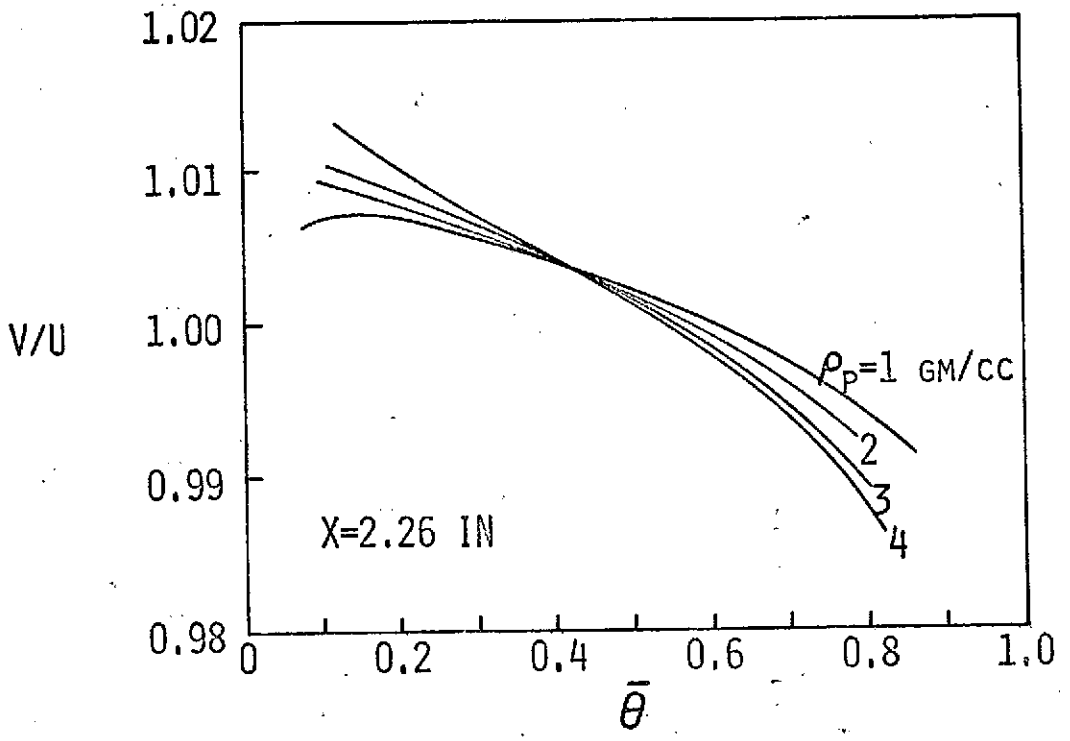
1.02
1.01
1.00
0.99
0.98
V/U
ρ_p=1 GM/CC
2
3
4
X=2.26 IN
0
0.2
0.4
0.6
0.8
1.0
$\bar{\theta}$

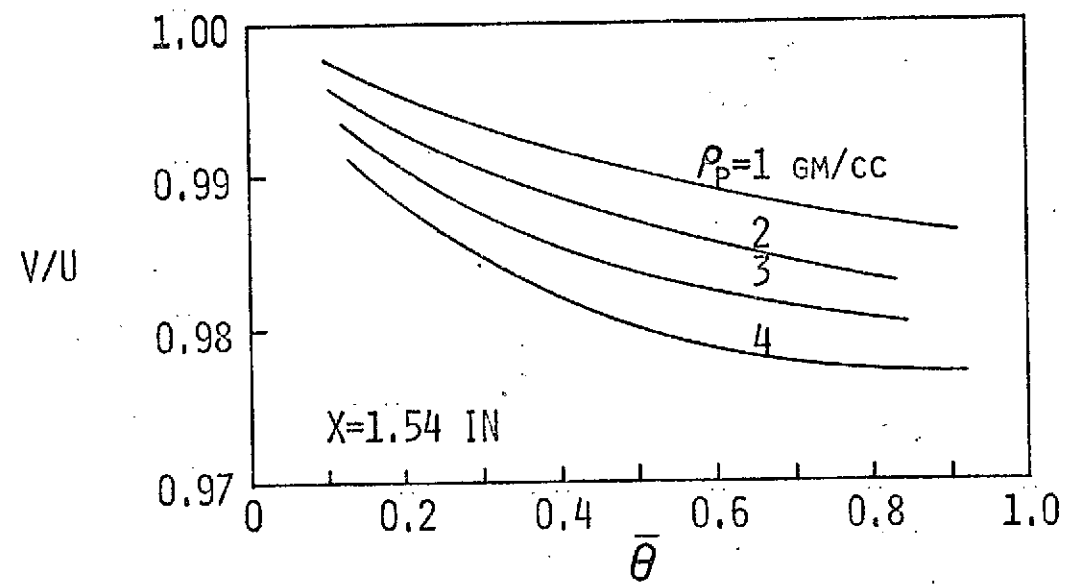
1.00
0.99
0.98
0.97
V/U
ρ_p=1 GM/CC
2
3
4
X=1.54 IN
0
0.2
0.4
0.6
0.8
1.0
$\bar{\theta}$

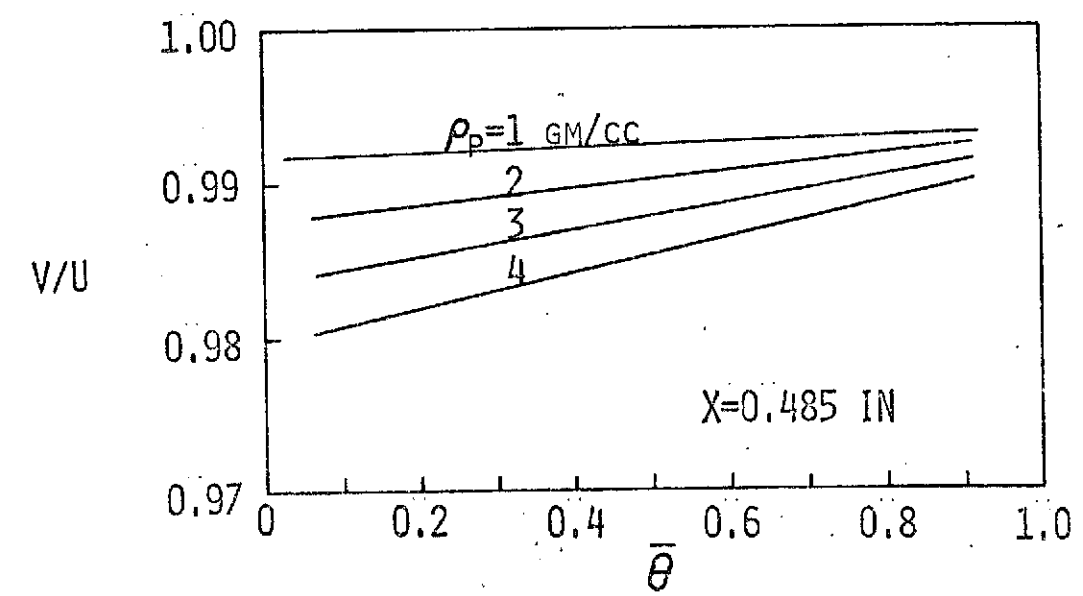
1.00
0.99
0.98
0.97
V/U
ρ_p=1 GM/CC
2
3
4
X=0.485 IN
0
0.2
0.4
0.6
0.8
1.0
$\bar{\theta}$

FIGURE 10

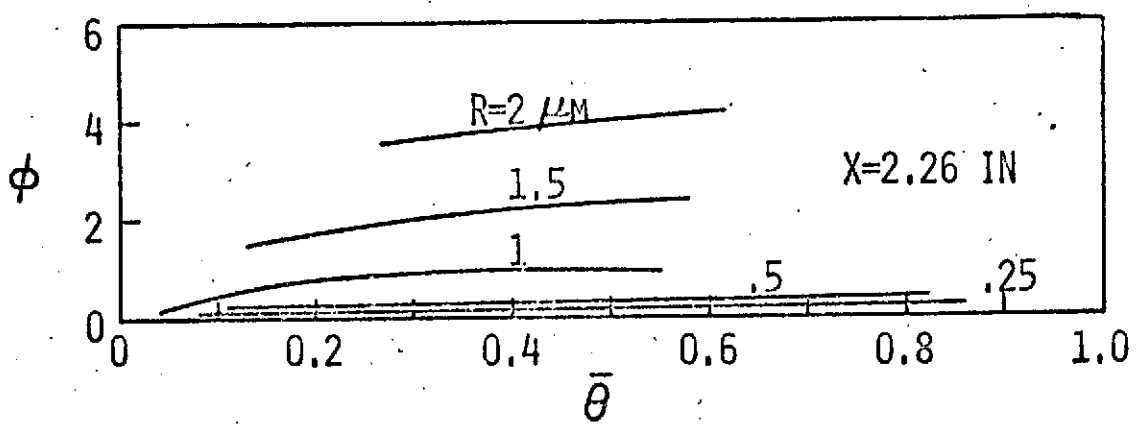
6
4
2
0
ϕ
R=2 μM
1.5
1
.5
.25
X=2.26 IN
0
0.2
0.4
0.6
0.8
1.0
$\bar{\theta}$

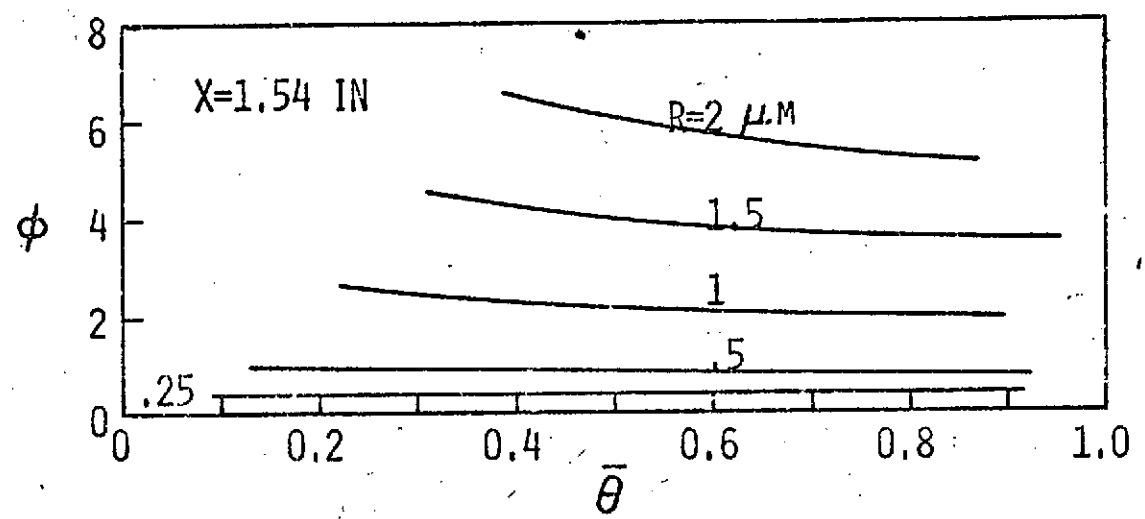
8
6
4
2
0
ϕ
X=1.54 IN
R=2 μM
1.5
1
.5
.25
0
0.2
0.4
0.6
0.8
1.0
$\bar{\theta}$

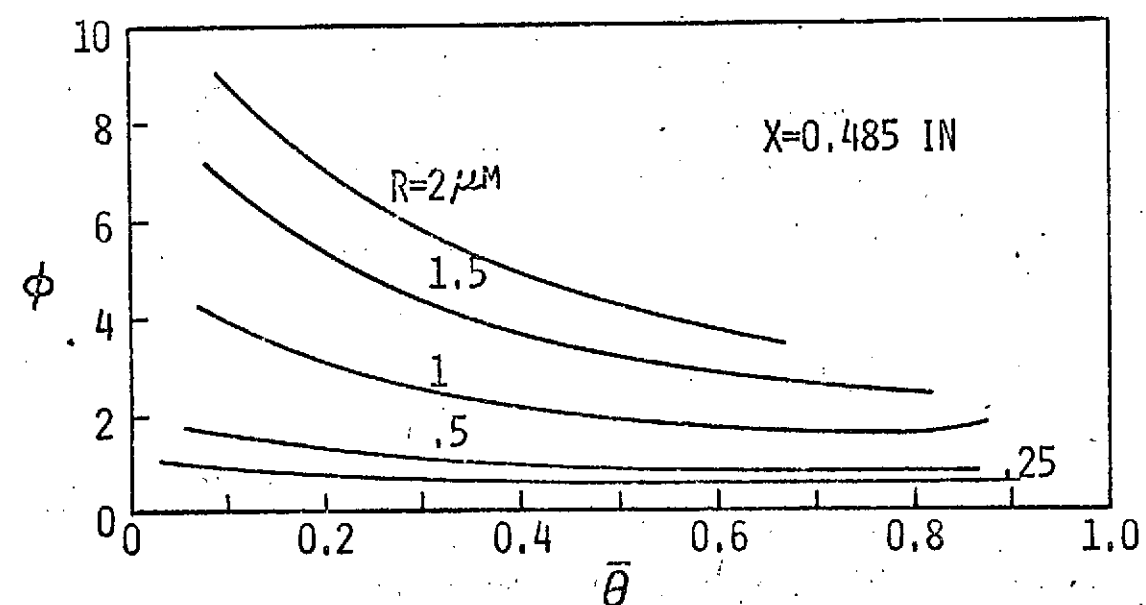
10
8
6
4
2
0
ϕ
X=0.485 IN
R=2 μM
1.5
1
.5
.25
0
0.2
0.4
0.6
0.8
1.0
$\bar{\theta}$

FIGURE 11

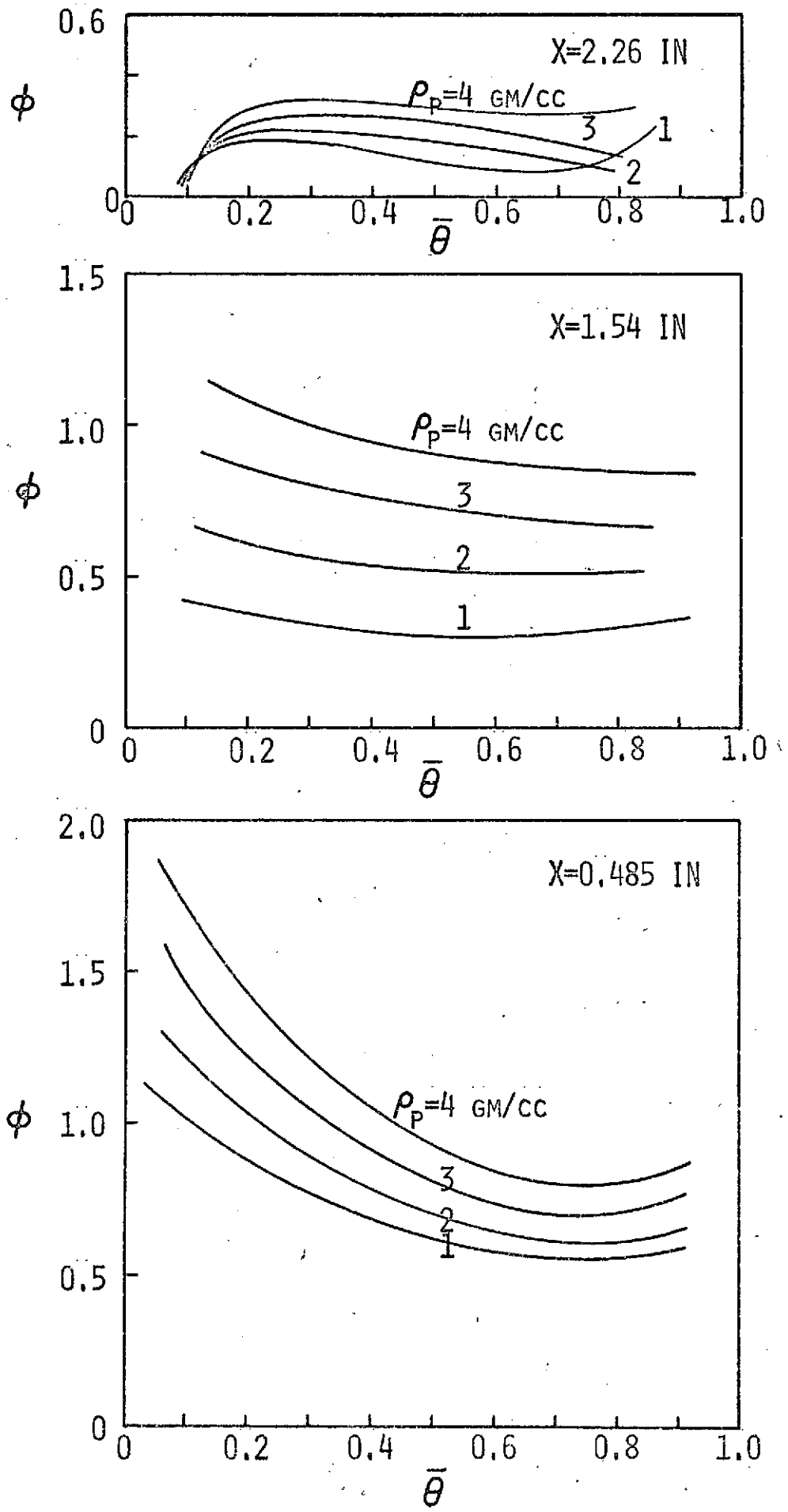
X=2.26 IN
ρ_p=4 GM/CC
3
1
2
ϕ
$\bar{\theta}$
0.6
0
0.2
0.4
0.6
0.8
1.0
X=1.54 IN
ρ_p=4 GM/CC
3
2
1
1.5
1.0
0.5
X=0.485 IN
ρ_p=4 GM/CC
3
2
1
2.0

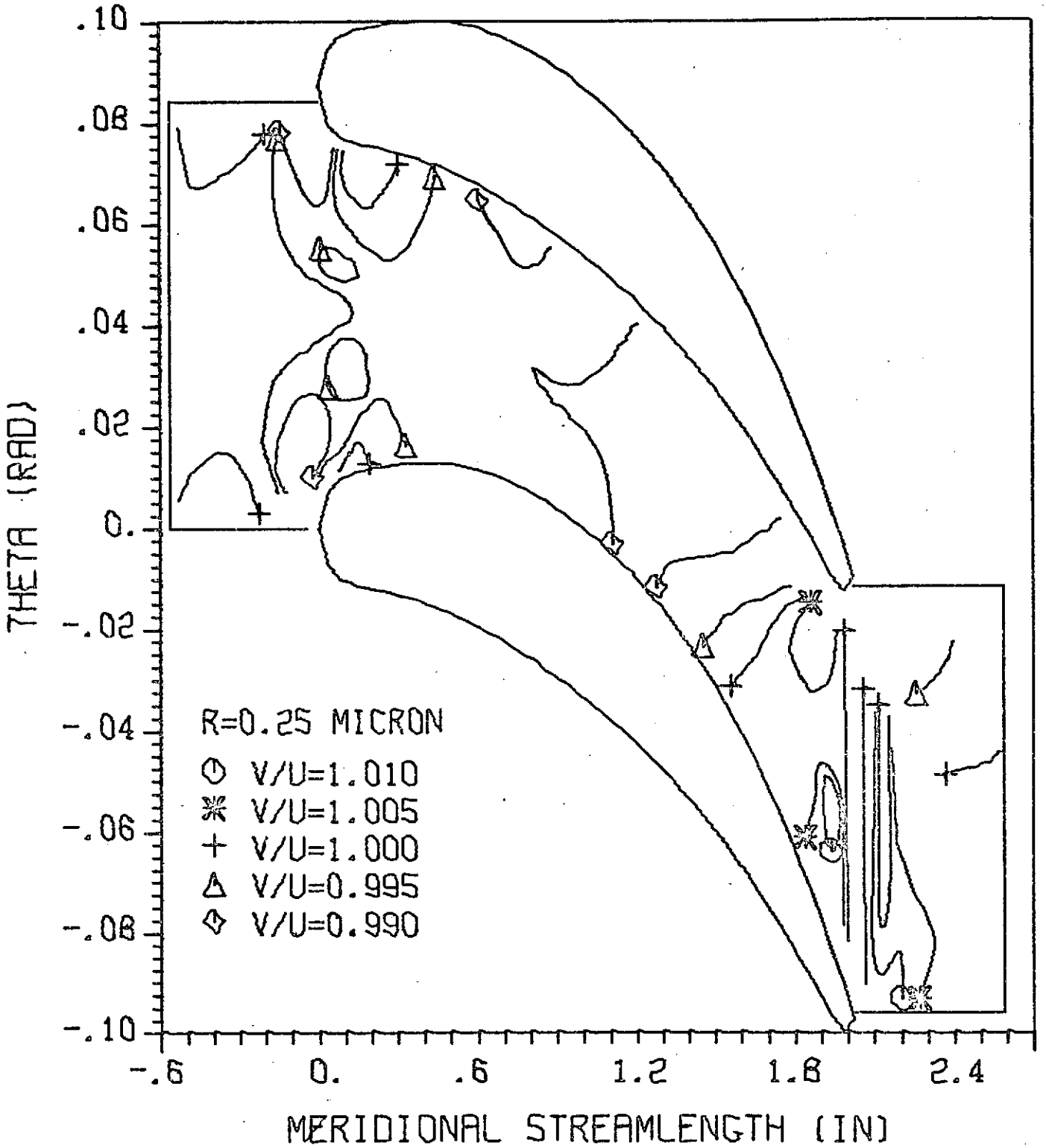

FIGURE 12A CONTOURS OF CONSTANT PARTICLE-TO-GAS VELOCITY RATIO, ρ_p = 1 gm/cc

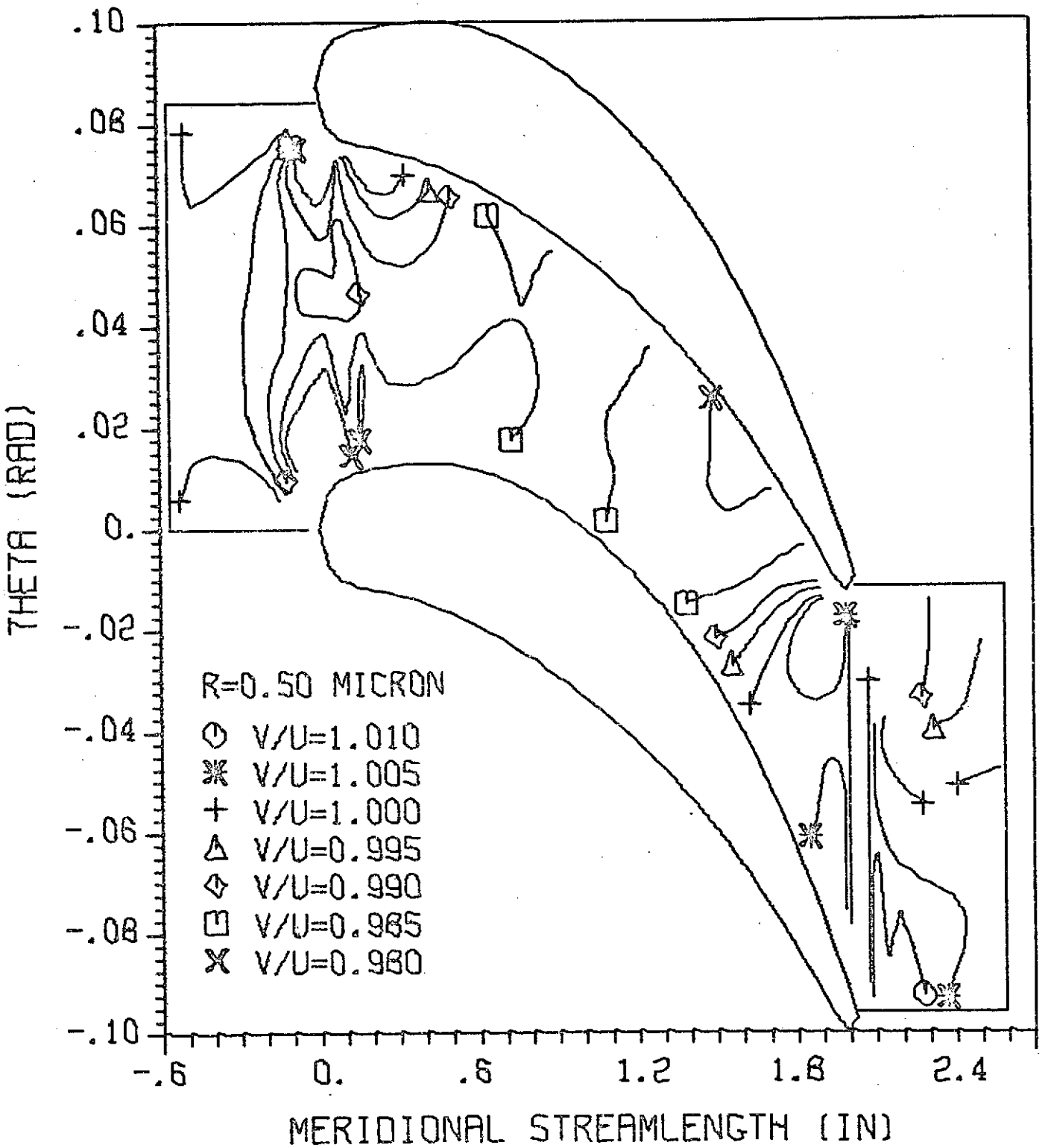

FIGURE 12B CONTOURS OF CONSTANT PARTICLE-TO-GAS VELOCITY RATIO, ρ_p = 1 gm/cc

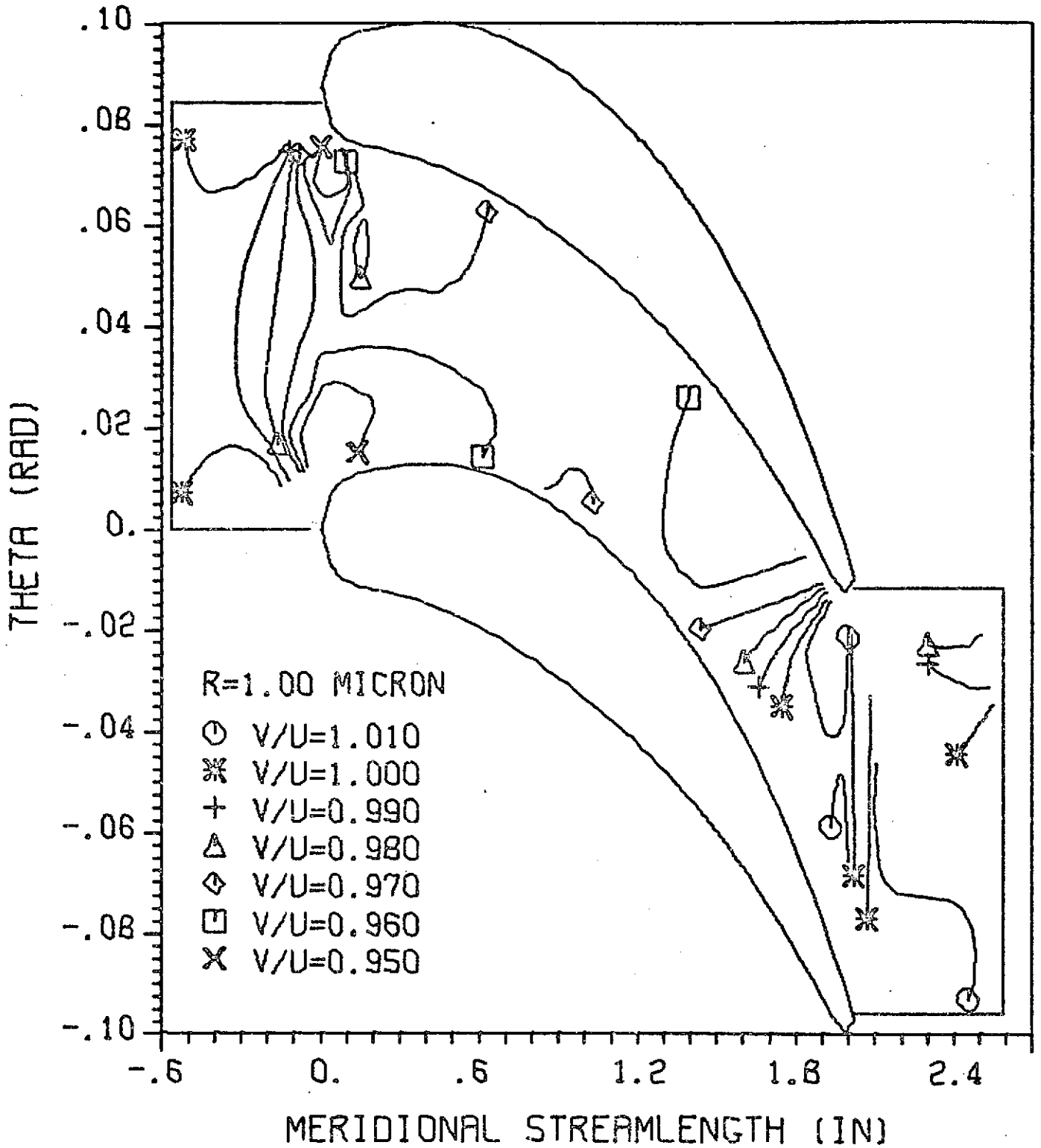

FIGURE 12c CONTOURS OF CONSTANT PARTICLE-TO-GAS VELOCITY RATIO, ρ_p = 1 gm/cc

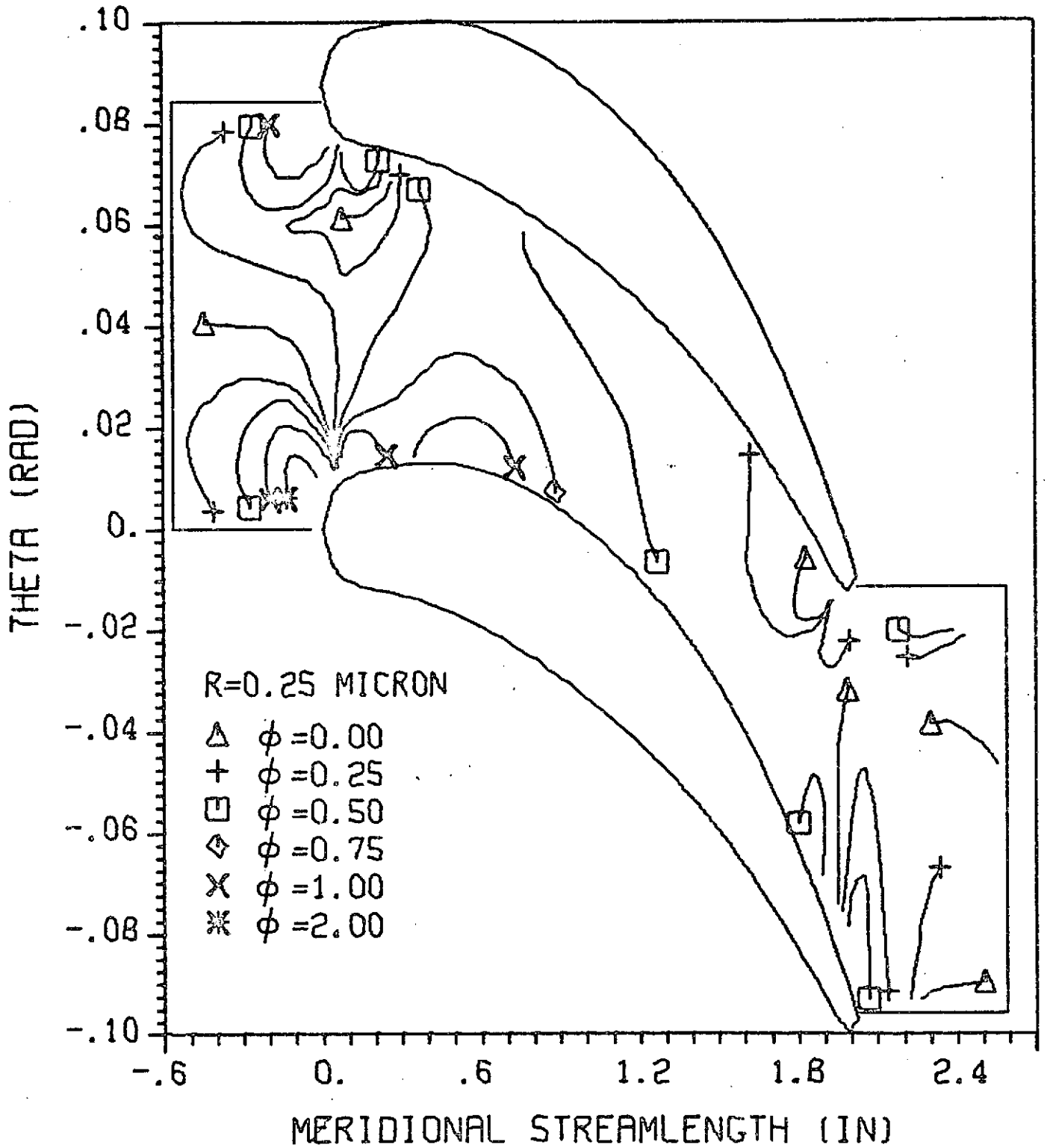

FIGURE 13A CONTOURS OF CONSTANT ANGULAR DEVIATION,

ρ_p = 1 gm/cc

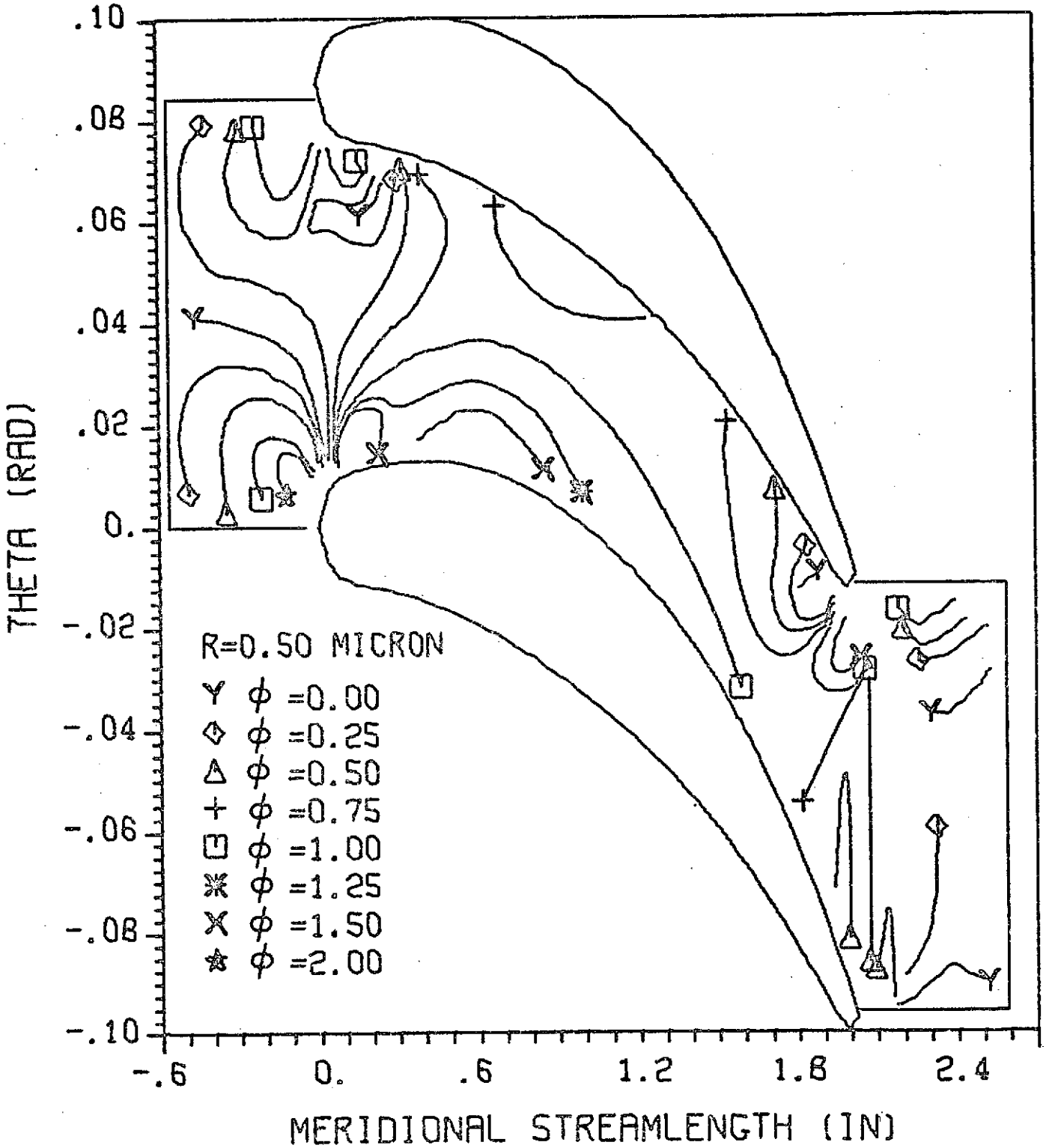

FIGURE 13B CONTOURS OF CONSTANT ANGULAR DEVIATION,

ρ_p = 1 gm/cc

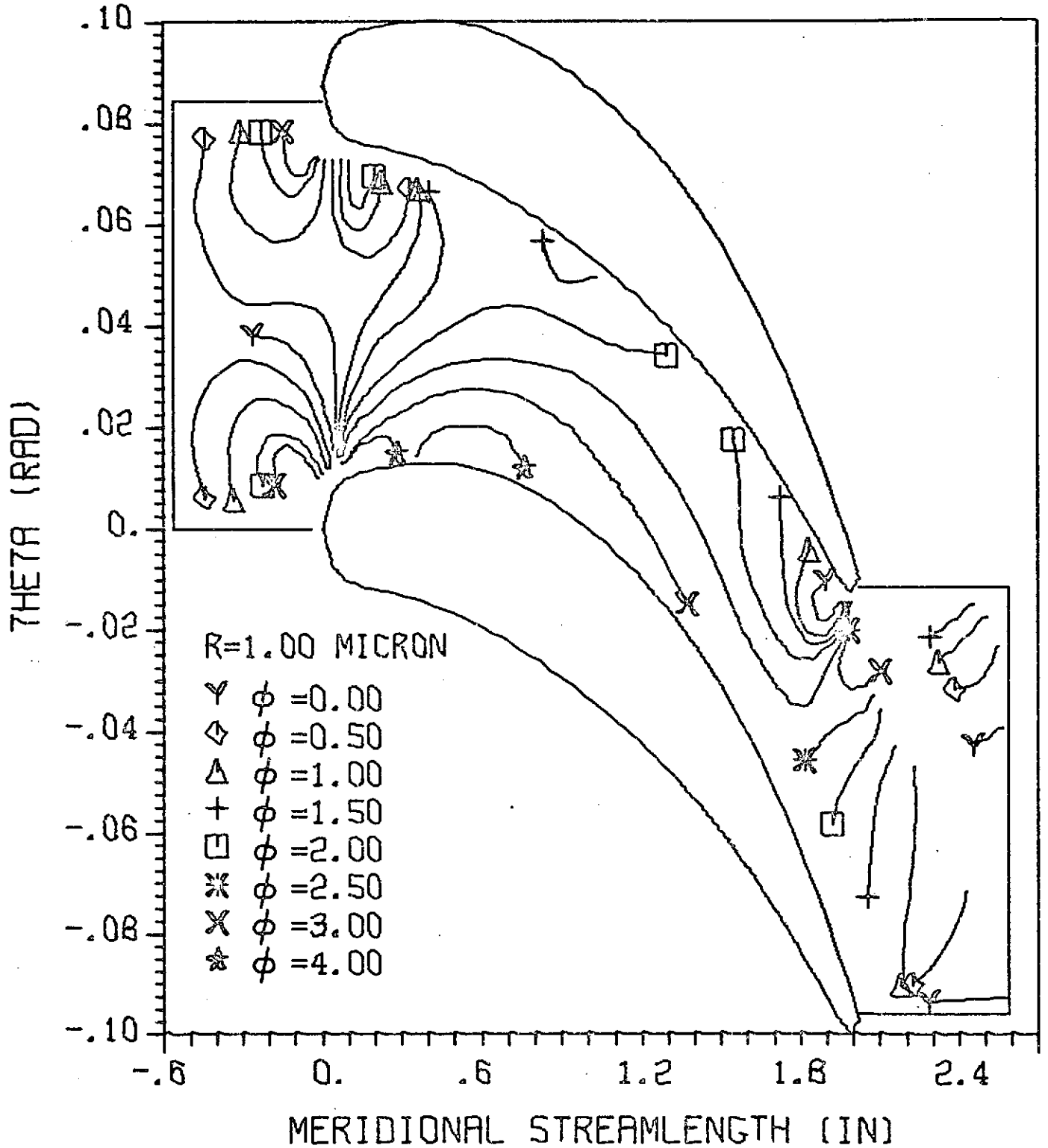

FIGURE 13c CONTOURS OF CONSTANT ANGULAR DEVIATION,

ρ_p = 1 gm/cc

Do not Print

REPORT DISTRIBUTION LIST FOR NASA CR-134543

Recipient	Address
Dr. Richard G. Seasholtz (3)	NASA Lewis Research Center 21000 Brookpark Road Cleveland, OH 44135 Mail Stop 77-1
Mr. Melvin J. Hartmann (1)	NASA Lewis Research Center 21000 Brookpark Road Cleveland, OH 44135 Mail Stop 5-9
Mr. Theodore Katsanis (1)	NASA Lewis Research Center 21000 Brookpark Road Cleveland, OH 44135 Mail Stop 77-2
Patent Counsel (1)	NASA Lewis Research Center 21000 Brookpark Road Cleveland, OH 44135 Attention: Norman T. Musial
Lewis Library (2)	NASA Lewis Research Center 21000 Brookpark Road Cleveland, OH 44135 Attention: Library
Lewis Technical Information Division (1)	NASA Lewis Research Center 21000 Brookpark Road Cleveland, OH 44135 Attention: Report Control Office
NASA Headquarters Technical information abstracting and dissemenation facility (6)	NASA Scientific and Technical Information Facility Box 5700 Bethesda, MD 20014 Attention: NASA Representative
Mr. Wayne Park (1)	NASA Lewis Research Center 21000 Brookpark Road Cleveland, OH 44135 Mail Stop 500-312